J|A|C|S
ARTICLES
Published on Web 08/28/2004

A Simple Thermodynamic Model for Rationalizing the Formation of Self-Assembled Multimetallic Edifices: Application to Triple-Stranded Helicates

Kornelia Zeckert,[†] Josef Hamacek,[†] Jean-Pierre Rivera,[†] Sébastien Floquet,[†,§] André Pinto,[‡] Michal Borkovec,[†] and Claude Piguet*,[†]

Contribution from the Department of Inorganic, Analytical, and Applied Chemistry, and Department of Organic Chemistry, University of Geneva, 30 quai E. Ansermet, CH-1211 Geneva 4, Switzerland

Received March 23, 2004; E-mail: Claude.Piguet@chiam.unige.ch

Abstract: Reaction of the bis-tridentate ligand bis{1-ethyl-2-[6′-(*N*,*N*-diethylcarbamoyl)pyridin-2′-yl]benzimidazol-5-yl}methane (L2) with $Ln(CF_3SO_3)_3 \cdot xH_2O$ in acetonitrile (Ln = La−Lu) demonstrates the successive formation of three stable complexes $[Ln(L2)_3]^{3+}$, $[Ln_2(L2)_3]^{6+}$, and $[Ln_2(L2)_2]^{6+}$. Crystal-field independent NMR methods establish that the crystal structure of $[Tb_2(L2)_3]^{6+}$ is a satisfying model for the helical structure observed in solution. This allows the qualitative and quantitative (β_{23}^{bi,Ln^1Ln^2}) characterization of the heterobimetallic helicates $[(Ln^1)(Ln^2)(L2)_3]^{6+}$. A simple free energy thermodynamic model based on (i) an absolute affinity for each nine-coordinate lanthanide occupying a terminal N_6O_3 site and (ii) a single intermetallic interaction between two adjacent metal ions in the complexes (ΔE) successfully models the experimental macroscopic constants and allows the rational molecular programming of the extended trimetallic homologues $[Ln_3(L5)_3]^{9+}$.

Introduction

During the past decade, helicates have been intensively investigated as the archetype of polymetallic supramolecular self-assembled edifices.[1] Major interest has been focused on the design of homotopic ligands, which provides homopolymetallic helicates existing as a single pair of enantiomers.[1] However, it was recognized early that the selective formation of heterometallic helicates requires different coordination sites provided by the use of heterotopic ligands possessing various binding units along their strands.[2] In this context, the design of heterobimetallic d−d[3] and d−f[4] helicates takes advantage of the specific stereochemical preferences of the metal ions, while the preparation of heterometallic f−f helicates remains challenging because of the great similitude of the complexation properties of the trivalent lanthanides, Ln(III), along the series. However, potential applications of molecular heteropolymetallic f−f assemblies in optics (upconversion,[5] downconversion,[6] signaling, and probing),[7] magnetism,[8] and catalysis[9] require efficient methodologies for the selective introduction of trivalent lanthanides into predetermined sites. Interestingly, the first isolated triple-stranded helicates $[Ln_2(L1)_3]^{6+}$ exhibited some deviations from the binomial statistical distribution, which disfavored the formation of the heterobimetallic complexes $[(Ln^1)(Ln^2)(L1)_3]^{6+}$,[10] a phenomenon not detected for the

[†] Department of Inorganic Chemistry, University of Geneva.
[‡] Department of Organic Chemistry, University of Geneva.
[§] Current address: Institut Lavoisier, Université de Versailles Saint Quentin, 45 av. des Etats-Unis, 78035 Versailles, France.

(1) (a) Constable, E. C. *Tetrahedron* **1992**, *48*, 10013. (b) Constable, E. C. *Prog. Inorg. Chem.* **1994**, *42*, 67. (c) Constable, E. C. In *Comprehensive Supramolecular Chemistry*; Atwood, J. L., Davies, J. E. D., MacNicol, D. D., Vögtle, F., Eds.; Pergamon: Oxford, 1996; Chapter 6. (d) Piguet, C.; Bernardinelli, G.; Hopfgartner, G. *Chem. Rev.* **1997**, *97*, 2005. (e) Albrecht, M. *Chem. Rev.* **2001**, *101*, 3457.
(2) (a) Constable, E. C.; Heirtzler, F.; Neuburger, M.; Zehnder, M. *J. Am. Chem. Soc.* **1997**, *119*, 5606. (b) Albrecht, M. *Chem. Soc. Rev.* **1998**, *27*, 281. (c) Greenwald, M.; Wessely, D.; Goldberg, I.; Cohen, Y. *New J. Chem.* **1999**, 337. (d) Hannon, M. J.; Bunce, S.; Clarke, A. J.; Alcock, N. W. *Angew. Chem., Int. Ed.* **1999**, *38*, 1277. (e) Mathieu, J.; Marsura, A.; Bouhmaida, N.; Ghermani, N. *Eur. J. Inorg. Chem.* **2002**, 2433.
(3) (a) Constable, E. C.; Edwards, A. J.; Raithby, R.; Walker, J. V. *Angew. Chem., Int. Ed. Engl.* **1993**, *32*, 1465. (b) Piguet, C.; Hopfgartner, G.; Bocquet, B.; Schaad, O.; Williams, A. F. *J. Am. Chem. Soc.* **1994**, *116*, 9092. (c) Smith, V. C.; Lehn, J.-M. *Chem. Commun.* **1996**, 2733.
(4) (a) Piguet, C.; Bünzli, J.-C. G.; Bernardinelli, G.; Hopfgartner, G.; Petoud, S.; Schaad, O. *J. Am. Chem. Soc.* **1996**, *118*, 6681. (b) Piguet, C.; Rivara-Minten, E.; Bernardinelli, G.; Bünzli, J.-C. G.; Hopfgartner, G. *J. Chem. Soc., Dalton Trans.* **1997**, 421. (c) Piguet, C.; Edder, C.; Rigault, S.; Bernardinelli, G.; Bünzli, J.-C. G.; Hopfgartner, G. *J. Chem. Soc., Dalton Trans.* **2000**, 3999. (d) Rigault, S.; Piguet, C.; Bernardinelli, G.; Hopfgartner, G. *J. Chem. Soc., Dalton Trans.* **2000**, 4587. (e) Cantuel, M.; Bernardinelli, G.; Imbert, D.; Bünzli, J.-C. G.; Hopfgartner, G.; Piguet, C. *J. Chem. Soc., Dalton Trans.* **2002**, 1929.
(5) (a) Gamelin, D. R.; Güdel, H. U. *Acc. Chem. Res.* **2000**, *33*, 235. (b) Auzel, F. *Chem. Rev.* **2004**, *104*, 139.
(6) (a) Wegh, R. T.; Donker, H.; Oskam, K. D.; Meijerink, A. *J. Luminesc.* **1999**, *82*, 93. (b) Ronda, C. *J. Luminesc.* **2002**, *100*, 301.
(7) (a) Bünzli, J.-C. G.; Piguet, C. *Chem. Rev.* **2002**, *102*, 1897. (b) Faulkner, S.; Pope, S. J. A. *J. Am. Chem. Soc.* **2003**, *125*, 10526. (c) Pope, S. J. A.; Kenwright, A. M.; Boote, V. A.; Faulkner, S. *Dalton Trans.* **2003**, 3780.
(8) (a) Ishikawa, N.; Iino, T.; Kaizu, Y. *J. Am. Chem. Soc.* **2002**, *124*, 11440. (b) Costes, J.-P.; Nicodème, F. *Chem.−Eur. J.* **2002**, *8*, 3442. (c) Costes, J.-P.; Dahan, F.; Nicodème, F. *Inorg. Chem.* **2003**, *42*, 6556. (d) Nicolle, G. M.; Yerly, F.; Imbert, D.; Böttger, U.; Bünzli, J.-C. G.; Merbach, A. E. *Chem.−Eur. J.* **2003**, *9*, 5453.
(9) (a) Hurst, P.; Takasaki, B. K.; Chin, J. *J. Am. Chem. Soc.* **1996**, *118*, 9982. (b) Pratviel, G.; Bernardou, J.; Meunier, B. *Adv. Inorg. Chem.* **1998**, *45*, 251. (c) Komiyama, M.; Takeda, N.; Shigekawa, H. *Chem. Commun.* **1999**, 1443. (d) Zheng, Z. *Chem. Commun.* **2001**, 2251. (e) Liu, C.; Wang, M.; Zhang, T.; Sun, H. *Coord. Chem. Rev.* **2004**, *248*, 147.
(10) Piguet, C.; Bünzli, J.-C. G.; Bernardinelli, G.; Hopfgartner, G.; Williams, A. F. *J. Am. Chem. Soc.* **1993**, *115*, 8197.

Chart 1

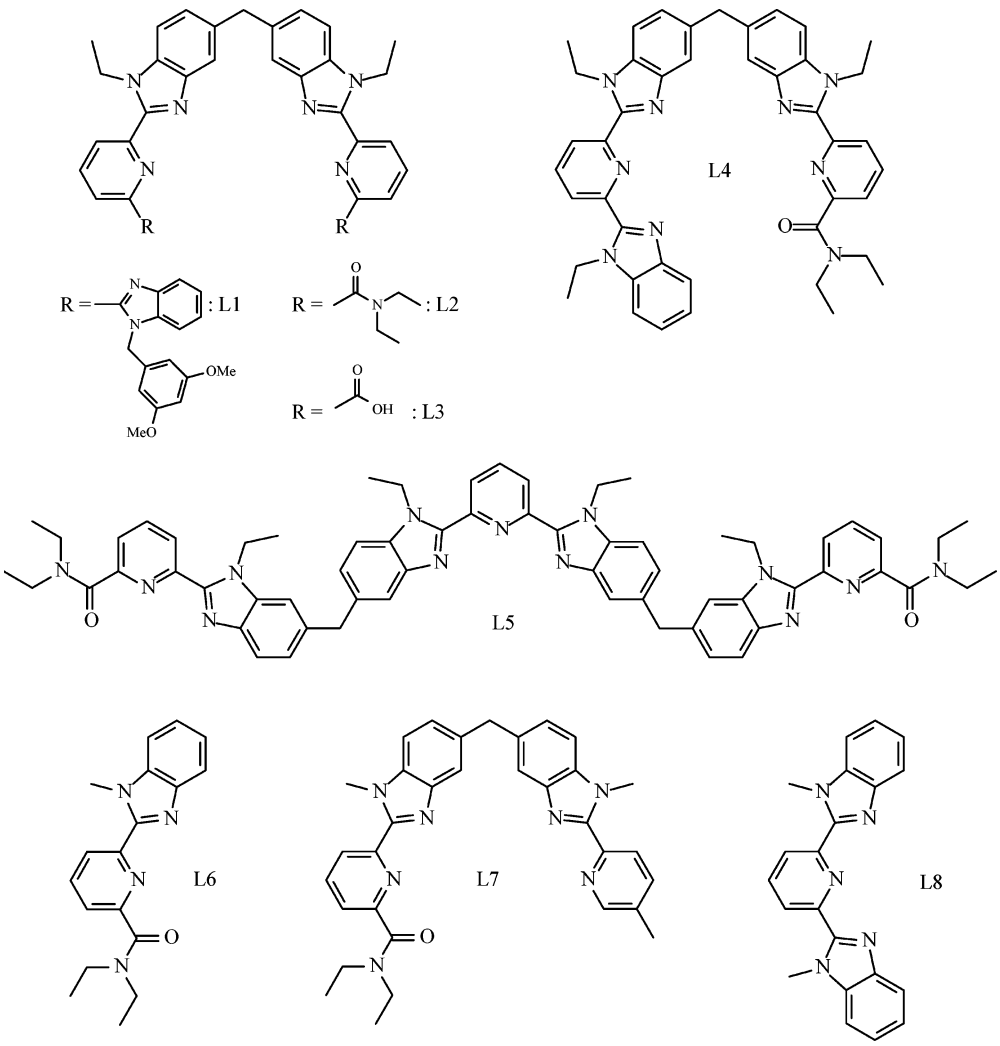

analogous helicates $[(Ln^1)(Ln^2)(L2)_3]^{6+}$.[11] As an attempt to improve selectivity, two different tridentate binding units have been introduced into the heterotopic ligand L4, which reacts with Ln(III) to give mixtures of C_3-symmetrical *HHH*-$[Ln_2(L4)_3]^{6+}$ and C_1-symmetrical *HHT*-$[Ln_2(L4)_3]^{6+}$ isomers. Fortunately, the use of two Ln(III) of sufficiently different size simultaneously favors (i) the formation of the head-to-head-to-head isomer (i.e., *HHH*) and (ii) the selective introduction of the smallest Ln(III) into the N_6O_3 site in *HHH*-$[(Ln^1)(Ln^2)(L4)_3]^{6+}$.[12] Although the origin of this nonpredicted thermodynamic effect remains obscure, its rationalization is a prerequisite for further programming heterometallic f−f helicates. As a first step toward this goal, a simple thermodynamic model has been developped for the D_3-symmetrical trimetallic triple-stranded helicates $[Ln_3(L5)_3]^{9+}$, which possess two equivalent nonadentate terminal N_6O_3 sites (t) and one central nonadentate N_9 site (c) (Figure 1).[13] In this *site-binding* model, the helicates are considered as preassembled one-dimensional receptors in which n metallic sites are available for the complexation of Ln(III). The free energy of complexation for each specific site is given by $\Delta G^{Ln}_{site\,i} = -RT\ln(k_i^{Ln})$, in which k_i^{Ln} corresponds to the absolute affinity constant of site i for Ln, and a single free energy parameter $\Delta E_{Ln^1Ln^2}$ describes the intermetallic interaction between two adjacent metal ions.[13] Application of this model for the assembly of $[Ln_3(L5)_3]^{9+}$ shows that the total free energy change ΔG_{tot} associated with the formation of the trimetallic helicates thus amounts to $\Delta G_{tot} = -2RT\ln(k_t^{Ln}) - RT\ln(k_c^{Ln}) + 2\Delta E_{LnLn} = -RT\ln(\beta_{33}^{LnLnLn})$. This translates into $\beta_{33}^{LnLnLn} = (k_t^{Ln})^2 \cdot k_c^{Ln} \cdot (e^{-(\Delta E_{LnLn}/RT)})^2 = (k_t^{Ln})^2 \cdot k_c^{Ln} \cdot (u_{LnLn})^2$ in which β_{33}^{LnLnLn} is the experimental macroscopic formation constant of $[Ln_3(L5)_3]^{9+}$ and u_{LnLn} is a *Boltzmann*'s factor representing the intermetallic interaction.[13,14] Although this approach neglects the explicit separation of intermolecular and intramolecular thermodynamic steps responsible for the assembly of the final helicates,[15] the formation constants and experimental distributions of the homo- and heterotrimetallic complexes $[(Ln^1)_x(Ln^2)_{3-x}(L5)_3]^{9+}$ ($x = 0-3$) in acetonitrile could be satisfyingly modeled.[13] However, the limited set of available macroscopic constants for these trimetallic helicates (i.e., a maximum of six for each Ln^1/Ln^2 pair)[13]

(11) Martin, N.; Bünzli, J.-C. G.; McKee, V.; Piguet, C.; Hopfgartner, G. *Inorg. Chem.* **1998**, *37*, 577.
(12) André, N.; Jensen, T. B.; Scopelliti, R.; Imbert, D.; Elhabiri, M.; Hopfgartner, G.; Piguet, C.; Bünzli, J.-C. G. *Inorg. Chem.* **2004**, *43*, 515.
(13) (a) Floquet, S.; Ouali, N.; Bocquet, B.; Bernardinelli, G.; Imbert, D.; Bünzli, J.-C. G.; Hopfgartner, G.; Piguet, C. *Chem.—Eur. J.* **2003**, *9*, 1860. (b) Floquet, S.; Borkovec, M.; Bernardinelli, G.; Pinto, A.; Leuthold, L.-A.; Hopfgartner, G.; Imbert, D.; Bünzli, J.-C. G.; Piguet, C. *Chem.—Eur. J.* **2004**, *10*, 1091.
(14) Koper, G.; Borkovec, M. *J. Phys. Chem. B* **2001**, *105*, 6666.
(15) Ercolani, G. *J. Am. Chem. Soc.* **2003**, *125*, 16097.

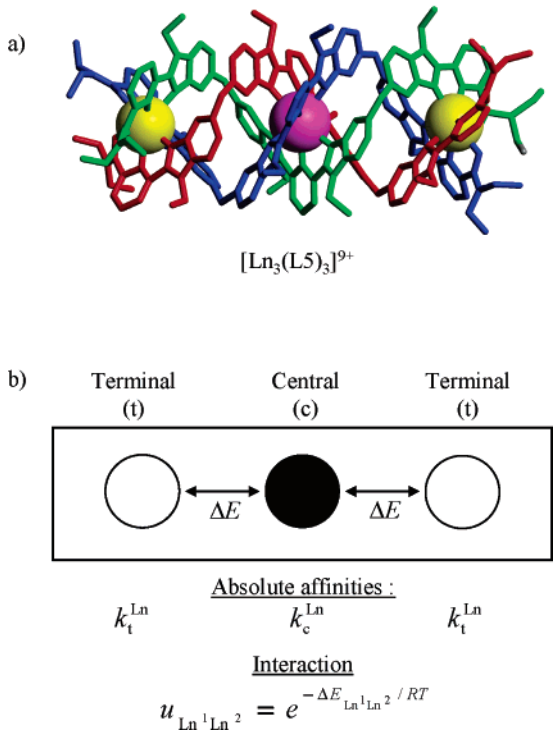

Figure 1. (a) Crystal structure of $[Eu_3(L5)_3]^{9+}$ and (b) associated thermodynamic *site-binding* model.[13]

prevents a complete analysis of the origin of any recognition processes because $\Delta E_{Ln^1Ln^2}$ was arbitrarily set to zero.[13]

In this paper, we put the basis for the complete quantitative modeling of the formation of multimetallic helicates. The detailed structural and thermodynamic characterization of the assembly process leading to $[Ln_2(L2)_3]^{6+}$ provides an initial set of absolute affinities for the terminal N_6O_3 site, together with acceptable intermetallic interactions. Subsequent global fits incorporating data collected for both bimetallic and trimetallic helicates eventually establish reliable absolute affinities for the pseudo-tricapped trigonal prismatic N_6O_3 and N_9 sites.

Results and Discussion

Thermodynamic Self-Assembly of the Homobimetallic Triple-Stranded Helicates $[Ln_2(L2)_3]^{6+}$ (Ln = La−Lu, except Pm). Previous partial investigations of the reaction of L2 with $Ln(CF_3SO_3)_3 \cdot xH_2O$ in acetonitrile (Ln = La, Eu, Gd, Tb, Lu) suggest that (i) stable triple-stranded helicates $[Ln_2(L2)_3]^{6+}$ are formed for a stoichiometric ratio Ln/L2 = 0.67 and (ii) these helicates are destroyed in an excess of metal to give the side-by-side bimetallic complexes $[Ln_2(L2)_2]^{6+}$ (Figure 2).[11] Surprisingly, no intermediate displaying a stoichiometric ratio Ln/L2 < 0.67 could be evidenced,[11] which strongly contrasts with the formation of the unsaturated complexes $[Ln_2(L5)_3]^{6+}$ during the assembly of the related trimetallic helicates $[Ln_3(L5)_3]^{9+}$.[13]

We have thus performed a thorough reinvestigation of the complexation properties of L2 with Ln(III) along the complete lanthanide series (Ln = La−Lu, except Pm). ESI-MS titrations of L2 (2×10^{-4} M) with $Ln(CF_3SO_3)_3 \cdot xH_2O$ in acetonitrile for ratios 0.1−1.1 show the successive formation of $[Ln(L2)_3(CF_3SO_3)_m]^{(3-m)+}$ ($m = 0, 1$), $[Ln_2(L2)_3(CF_3SO_3)_m]^{(6-m)+}$ ($m = 0-4$), and $[Ln_2(L2)_2(CF_3SO_3)_m]^{(6-m)+}$ ($m = 2-5$) (Table S1, Supporting Information). The two latter complexes match our original suggestion,[11] but the systematic observation in the gas phase of the monometallic complexes $[Ln(L2)_3(CF_3SO_3)_m]^{(3-m)+}$ in considerable proportions for Ln/L2 < 0.67 strongly suggests its existence in solution. Parallel spectrophotometric titrations of L2 with $Ln(CF_3SO_3)_3 \cdot xH_2O$ in the same conditions show a complicated variation of the UV spectra resulting from the trans−trans → cis−cis isomerization of the tridentate binding units occurring upon complexation (Figure 3a).[4a] Two smooth end points are detected about Ln/L2 = 2:3 and Ln/L2 = 1:1, together with some weak inflection around Ln/L2 = 1:3 (Figure 3b). Factor analysis[16] systematically confirms the formation of four absorbing species assigned to L2, $[Ln(L2)_3]^{3+}$, $[Ln_2(L2)_3]^{6+}$,

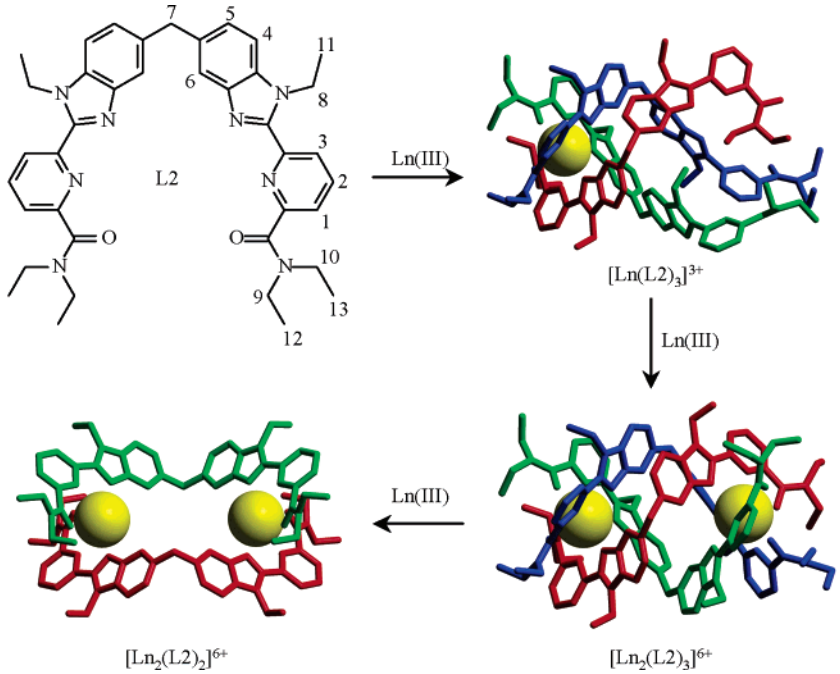

Figure 2. Complexation properties of L2 with Ln(III) in acetonitrile. The structures of $[Ln_2(L2)_3]^{6+}$ and $[Ln_2(L2)_2]^{6+}$ correspond to the crystal structures found for $[Tb_2(L2)_3]^{6+}$ and $[(Eu(CF_3SO_3)_2OH_2)_2(L2)_2]^{2+}$, respectively (the coordinated triflates and water molecules have been omitted for clarity).[11]

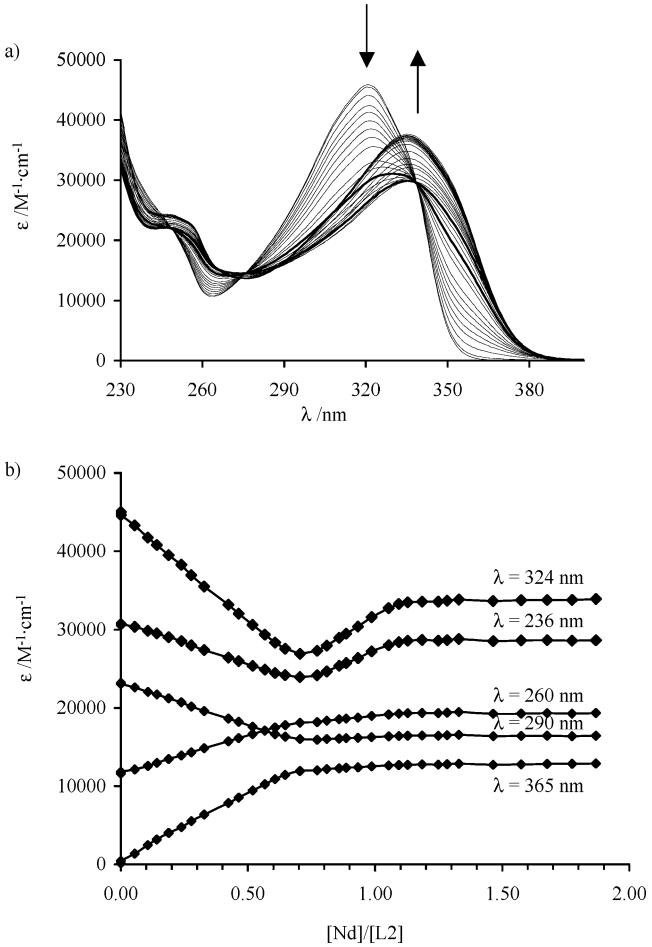

Figure 3. (a) Variation of absorption spectra observed for the spectrophotometric titration of L2 (2×10^{-4} M in acetonitrile) with $Nd(CF_3SO_3)_3 \cdot 2H_2O$ at 298 K (Nd/L2 = 0−1.9). (b) Corresponding variations of observed molar extinctions at five different wavelengths.

and $[Ln_2(L2)_2]^{6+}$ in complete agreement with ESI-MS data. The spectrophotometric data can be satisfyingly fitted with nonlinear least-squares techniques[17] to equilibria 1−3, and the associated formation constants are collected in Table 1.

$$Ln^{3+} + 3L2 \rightleftharpoons [Ln(L2)_3]^{3+} \quad \log(\beta_{13}^{bi,Ln}) \qquad (1)$$

$$2\,Ln^{3+} + 3L2 \rightleftharpoons [Ln_2(L2)_3]^{6+} \quad \log(\beta_{23}^{bi,LnLn}) \qquad (2)$$

$$2\,Ln^{3+} + 2L2 \rightleftharpoons [Ln_2(L2)_2]^{6+} \quad \log(\beta_{22}^{bi,LnLn}) \qquad (3)$$

Although $\log(\beta_{13}^{bi,Ln})$ and $\log(\beta_{22}^{bi,LnLn})$ display no significant variations along the lanthanide series within experimental error (Table 1 and Figure S1, Supporting Information), $\log(\beta_{23}^{bi,LnLn})$ versus the inverse of the ionic radii of nine-coordinate Ln(III)[18] exhibits a concave bowl-shaped curve with a maximum around the middle of the lanthanide series (Figure 10a and Figure S1, Supporting Information). This observation is reminiscent of a similar trend reported for the same terminal nonadentate N_6O_3 site in $[Ln_3(L5)_3]^{9+}$,[13] but it contrasts with the smooth classical

Table 1. Formation Constants $\log(\beta_{mn}^{Bi,Ln})$ Obtained by Spectrophotometry for the Complexes $[Ln_m(L2)_n]^{3m+}$ (Ln = La−Lu, Y; m = 1, 2; n = 2, 3; Acetonitrile, 298 K)[a]

Ln(III)	$r_{Ln}^{CN=9}$/Å[b]	$\log(\beta_{13}^{bi,Ln})$	$\log(\beta_{13}^{bi,calc})$[c]	$\log(\beta_{23}^{bi,LnLn})$	$\log(\beta_{23}^{bi,calc})$[c]	$\log(\beta_{22}^{bi,LnLn})$
La(III)	1.216	17.0(4)	17.2	25.1(2)	25.1	19.2(5)
Ce(III)	1.196	18.1(5)		25.0(2)		18.9(1)
Pr(III)	1.179	16.7(4)		25.3(2)		19.4(5)
Nd(III)	1.163	18.8(5)	18.0	25.4(2)	25.3	19.3(4)
Sm(III)	1.132	17.5(4)	17.6	25.9(2)	25.7	20.0(5)
Eu(III)	1.120	19.4(5)	18.5	26.0(2)	25.9	19.6(2)
Gd(III)	1.107	18.8(5)		26.0(2)		19.8(2)
Tb(III)	1.095	17.8(3)		26.0(5)		20.0(5)
Dy(III)	1.083	17.2(4)		25.0(5)		20.1(5)
Y(III)	1.075	17.2(4)	17.5	25.8(2)	25.8	19.6(5)
Ho(III)	1.072	18.7(5)		25.8(2)		19.6(2)
Er(III)	1.062	18.4(5)		25.6(3)		19.4(3)
Tm(III)	1.052	18.7(5)		25.6(3)		19.3(3)
Yb(III)	1.042	16.1(9)	16.9	25.4(2)	25.5	19.2(5)
Lu(III)	1.032	17.1(5)	17.4	25.4(5)	25.3	19.3(4)

[a] The quoted errors correspond to those estimated during the fitting process. [b] Ionic radius for nine-coordinate Ln(III).[18] [c] Calculated by using eqs 16 and 19 with k_t^{Ln} taken from Table 4 (ΔE = 51 kJ mol^{-1}).

electrostratic dependence recently reported for the monometallic model complexes $[Ln(L6)_3]^{3+}$ in the same conditions.[19]

Finally, ^{1}H NMR titrations of L2 (10^{-2} M in CD_3CN) with $La(CF_3SO_3)_3 \cdot 2H_2O$ confirm the quantitative formation of the D_3-symmetrical triple-stranded helicate $[La_2(L2)_3]^{6+}$ for La:L2 = 0.67 (Figure 4a),[11] and of the intermediate complex $[La(L2)_3]^{3+}$ for La:L2 = 0.33 (Figure 4b), in complete agreement with the expected speciations of the ligand calculated with equilibria 1−3 in these conditions (i.e. > 93%, Table 1).

Interestingly, the three coordinated tridentate binding units in $[La(L2)_3]^{3+}$ display a single set of 31 well-resolved signals implying 3-fold symmetry (Figure 4b). The observation of diastereotopic methylene protons for H8−H8′, H9−H9′, and H10−H10′ points to a blocked C_3 symmetry on the NMR time scale which is only compatible with the quantitative formation (>95%) of the facial complex *FAC*-$[La(L2)_3]^{3+}$ in which the three ligand strands adopt parallel orientations (Figure 2). The protons of the noncoordinated tridentate binding units in the latter complex appear as dynamically broadened signals (Figure 4b), whose resolution is significantly improved at higher temperature. The absence of coalescence between the signals for the coordinated and noncoordinated tridentate binding units excludes an alternative interpretation considering a 1:1 mixture of $[La_2(L2)_3]^{6+}$ and L2 (Figure S2, Supporting Information). Comparable results are obtained for the paramagnetic complexes $[Ln(L2)_3]^{3+}$ (Ln = Nd, Eu, Figure S3, Supporting Information), for which the protons of the coordinated tridentate units are strongly paramagnetically shifted, while those of the unbound units are less affected. For $[Eu(L2)_3]^{3+}$, numerous weak signals corresponding to a second species (<5%) are detected in the baseline (Figure S3b), a phenomenon which becomes more important along the lanthanide series, and culminates for $[Lu(L2)_3]^{3+}$ (Figure 4c). This second minor set of ^{1}H NMR signals is assigned to the formation of traces of the meridional C_1-symmetrical isomers *MER*-$[Ln(L2)_3]^{3+}$ in which the three ligands are not equivalent (i.e., one strand adopts the reverse orientation), as recently reported for the monometallic model complex $[Ln(L6)_3]^{3+}$.[19] Again, the VT-NMR spectra of [Lu-

(16) Malinowski, E. R.; Howery, D. G. *Factor Analysis in Chemistry*, Wiley: New York, Chichester, 1980.
(17) (a) Gampp, H.; Maeder, M.; Meyer, C. J.; Zuberbühler, A. *Talanta* **1986**, *33*, 943. (b) Gampp, H.; Maeder, M.; Meyer, C. J.; Zuberbühler, A. *Talanta* **1985**, *32*, 1133.
(18) Shannon, R. D. *Acta Crystallogr.* **1976**, *A32*, 751.
(19) Le Borgne, T.; Altmann, P.; André, N.; Bünzli, J.-C. G.; Bernardinelli, G.; Morgantini, P.-Y.; Weber, J.; Piguet, C. *Dalton Trans.* **2004**, 723.

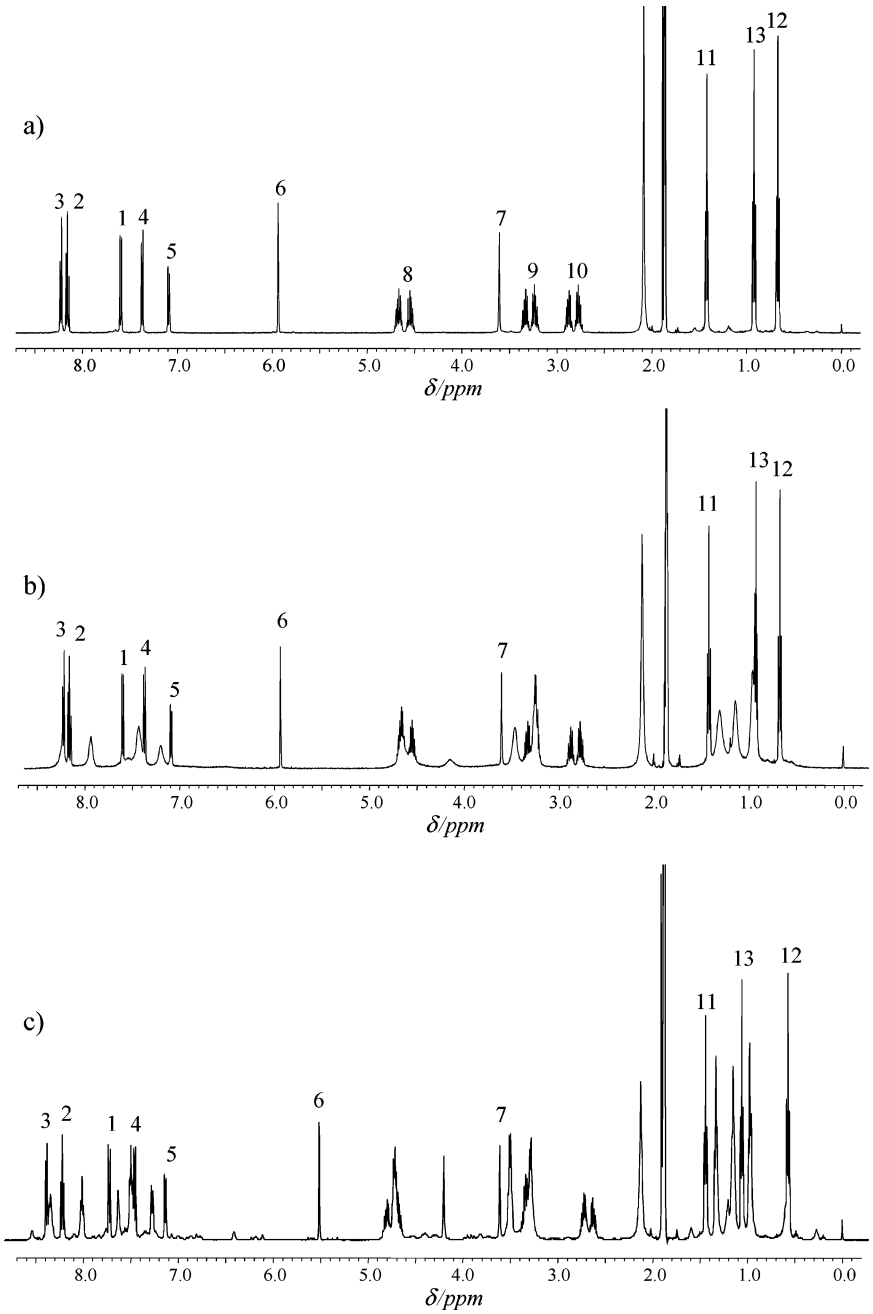

Figure 4. ^{1}H NMR spectra of (a) $[La_2(L2)_3]^{6+}$, (b) $[La(L2)_3]^{3+}$, and (c) $[Lu(L2)_3]^{3+}$ (CD_3CN, 298 K). Only the aromatic and methyl protons of the coordinated tridentate binding units are assigned (numbering scheme in Figure 2).

$(L2)_3]^{3+}$ point to a temperature-dependent dynamic process affecting the unbound tridentate units (Figure S4, Supporting Information). Finally, for Ln/L2 = 1.0, the triple-stranded helicates are destroyed to give the dynamically flexible $[Ln_2(L2)_2]^{6+}$ complexes (Ln = La, Nd, Eu, Lu), which display average D_{2h} symmetries on the NMR time scale.[11] From the combination of ESI-MS, spectrophotometric, and NMR titrations, we conclude that the assembly of the D_3-symmetrical triple-stranded helicates $[Ln_2(L2)_3]^{6+}$ implies the formation of the single thermodynamically stable intermediates $[Ln(L2)_3]^{3+}$, which exist almost exclusively as their facial isomers in solution. If the stoichiometric ratio Ln/L2 $\leq$ 0.67, the formation of the final side-by-side $[Ln_2(L2)_2]^{6+}$ complex can be neglected.

Solution Structure of the Homobimetallic Triple-Stranded Helicates $[Ln_2(L2)_3]^{6+}$ (Ln = La−Lu except Pm, Gd). For axial lanthanide complexes (i.e., possessing at least a C_3 or a C_4 axis), paramagnetic ^{1}H NMR spectroscopy is particularly well-suited for investigating isostructurality in solution along the lanthanide series,[20] a crucial point for a simple thermodynamic modeling of the formation of the D_3-symmetrical triple-stranded helicates $[Ln_2(L2)_3]^{6+}$. The paramagnetic NMR shift (δ_{ij}^{para}) of a magnetically active nucleus i is obtained from the experimental data (δ_{ij}^{exp}) by subtraction of the diamagnetic contribution (δ_i^{dia}) measured in the isostructural La, Y, or Lu

(20) (a) Peters, J. A.; Huskens, J.; Raber, D. J. *Prog. NMR Spectroscopy* **1996**, *28*, 283. (b) Forsberg, J. H. In *Handbook on the Physics and Chemistry of Rare Earths*; Gschneidner, K. A., Eyring, L., Eds.; Elsevier: Amsterdam, 1996; Vol. 23, Chapter 153, p 1. (c) Piguet, C.; Geraldes, C. F. G. C. In *Handbook on the Physics and Chemistry of Rare Earths*; Gschneidner, K. A., Jr., Bünzli, J.-C. G., Pecharsky, V. K., Eds.; Elsevier Science: Amsterdam, 2003; Vol. 33, Chapter 215, p 353.

Scheme 1. Axial Coordinates Considered in the Bimetallic D_3-symmetrical Complexes $[Ln_2(L2)_3]^{6+a}$

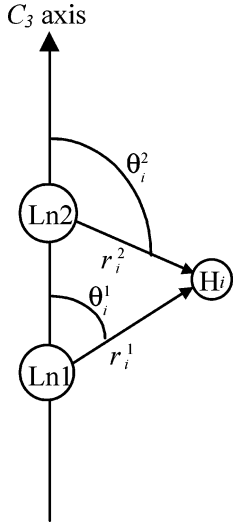

[a] Each Ln(III) is located at the origin of a specific polar frame.

complexes. It can be modeled with eq 4 assuming that the magnetic anisotropy produced by a lanthanide j, Ln^j, at room temperature is satisfyingly described by the second term of a power series in T^{-n} (high-temperature Bleaney's approximation),[20,21] F_i is the contact term (proportional to the Fermi constant A_i), $G_i = (3\cos^2\theta_i - 1)/r_i^3$ is the geometrical factor of the nucleus i (θ_i and r_i are the internal polar axial coordinates), $\langle S_z\rangle_j$ and C_j are, respectively, the spin expectation values[22] and Bleaney's factors[21] of the lanthanide j tabulated at 300 K, and B_0^2 is the second-rank crystal-field parameter measuring the effect of the specific location of the donor atoms in the first coordination sphere.[21]

$$\delta_{ij}^{\text{para}} = \delta_{ij}^{\text{exp}} - \delta_i^{\text{dia}} = \delta_{ij}^{\text{contact}} + \delta_{ij}^{\text{pseudo-contact}} = F_i\langle S_z\rangle_j + G_i B_0{}^2 C_j \quad (4)$$

For two magnetically noncoupled Ln(III) in $[Ln_2(L2)_3]^{6+}$,[23] eq 4 transforms into eq 5 (Scheme 1).[20c]

$$\delta_{ij}^{\text{para}} = F_i\langle S_z\rangle_j + (G_i^1 + G_i^2)B_0{}^2 C_j \quad (5)$$

The ^{1}H NMR spectra of $[Ln_2(L2)_3]^{6+}$ systematically show the 16 signals expected for homobimetallic D_3-symmetrical triple-stranded helicates, and this systematically corresponds to one-half of a L2 ligand (H8−H8′, H9−H9′, and H10−H10′ are diastereotopic, while H7−H7′ are enantiotopic).[1d,11] However, only the diamagnetic (Ln = La, Y, Lu) or the weakly paramagnetic (Ln = Ce−Eu) helicates possess nuclear relaxation times long enough to allow a reliable assignment of the six aromatic (H1−H6), eight methylene (H7−H10), and nine methyl (Me11−Me13) protons by using two-dimensional ^{1}H−^{1}H COSY and ^{1}H−^{1}H NOESY correlation spectra. For the strongly paramagnetic helicates (Ln = Tb−Yb), we have resorted to the determination of the longitudinal paramagnetic

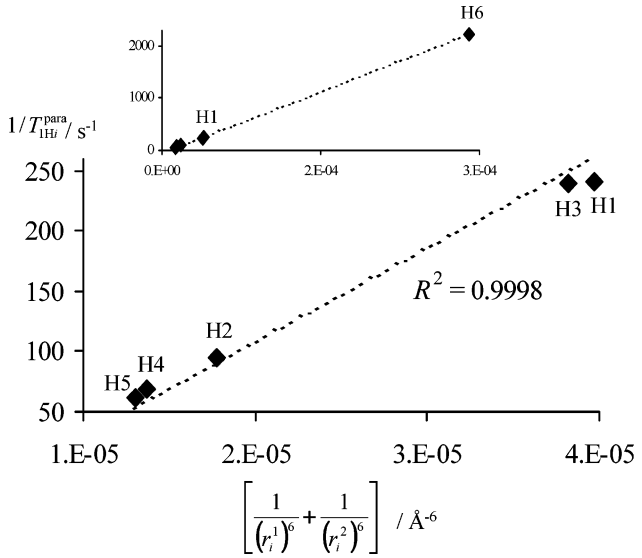

Figure 5. Plots of $1/T_{1i}^{\text{para}}$ vs $[1/(r_i^1)^6 + 1/(r_i^2)^6]$ according to eq 7 for H1−H6 in $[Tb_2(L2)_3]^{6+}$ (CD_3CN, 298 K, r_i^1 and r_i^2 are taken from the crystal structure of $[Tb_2(L2)_3]^{6+}$).[11]

relaxation rates $1/T_{1i}^{\text{para}} = 1/T_{1i}^{\text{exp}} - 1/T_{1i}^{\text{dia}}$ of Hi (i = 1−13). The latter are controlled by the transient and static (i.e., Curie spin) dipolar contributions which depend on complicated functions of the distances r_i^1 and r_i^2 separating Hi and the two magnetically equivalent lanthanide centers (eq 6, Scheme 1 and Table S2, Supporting Information).[13,20]

$$\frac{1}{T_{1i}^{\text{para}}} = \frac{4}{3}\left(\frac{\mu_0}{4\pi}\right)\gamma_I^2\mu_{\text{eff}}^4\beta^2\left[\frac{1}{(r_i^1)^6} + \frac{1}{(r_i^2)^6}\right]\tau_e + \frac{6}{5}\left(\frac{\mu_0}{4\pi}\right)^2\frac{\gamma_I^2\mu_{\text{eff}}^4\beta^4 H_0{}^2}{(3kT)^2}\left[\frac{1}{(r_i^1)^6} + \frac{1}{(r_i^2)^6}\right]\left(\frac{\tau_r}{1+\omega_I{}^2\tau_r{}^2}\right) \quad (6)$$

$$\frac{1}{T_{1i}^{\text{para}}} = K_j\left[\frac{1}{(r_i^1)^6} + \frac{1}{(r_i^2)^6}\right] \quad (7)$$

At fixed magnetic field and temperature, and for a given homobimetallic helicates containing the lanthanides j, eq 6 reduces to eq 7 in which K_j is a positive magnetic constant. We thus expect a straight line with a positive slope for plots of $1/T_{1i}^{\text{para}}$ *versus* $[1/(r_i^1)^6 + 1/(r_i^2)^6]$, r_i^1 and r_i^2 being estimated from the X-ray crystal structure of $[Tb_2(L2)_3]^{6+}$ (Scheme 1 and Table S3, Supporting Information).[11] For each paramagnetic complex $[Ln_2(L2)_3]^{6+}$, a single permutation of Hi provides a satisfying linear correlation, and the associated assignments are collected in Table S4 (Supporting Information) for Ln = Tb−Yb (Figure 5). As expected from previous work,[20c,23] the flexibility of the ethyl residues H8−H11, H9−H12, and H10−H13 prevents satisfying correlations between the solid state and solution structures, and we have thus focused our structural analysis on the six aromatic protons H1−H6 together with the enantiotopic methylene protons H7−H7′.

Transformation of eq 5 into its two linear forms (eqs 8 and 9) predicts that plots of $\delta_{ij}^{\text{para}}/\langle S_z\rangle_j$ vs $C_j/\langle S_z\rangle_j$ (eq 8) and $\delta_{ij}^{\text{para}}/C_j$ vs $\langle S_z\rangle_j/C_j$ (eq 9) are linear along an isostructural series of lanthanide complexes, assuming that the contact terms F_i and the crystal-field parameter B_0^2 are invariant (one-nucleus method).[20,23]

(21) (a) Bleaney, B. *J. Magn. Reson.* **1972**, *8*, 91. (b) Bleaney, B.; Dobson, C. M.; Levine, B. A.; Martin, R. B.; Williams, R. J. P.; Xavier, A. V. *J. Chem. Soc., Chem. Commun.* **1972**, 791. (c) Mironov, V. S.; Galyametdinov, Y. G.; Ceulemans, A.; Görller-Walrand, C.; Binnemans, K. *J. Chem. Phys.* **2002**, *116*, 4673.
(22) Golding, R. M.; Halton, M. P. *Aust. J. Chem.* **1972**, *25*, 2577.
(23) Elhabiri, M.; Scopelliti, R.; Bünzli, J.-C. G.; Piguet, C. *J. Am. Chem. Soc.* **1999**, *121*, 10747.

$$\frac{\delta_{ij}^{\text{para}}}{\langle S_z\rangle_j} = F_i + B_0^2(G_i^1 + G_i^2)\frac{C_j}{\langle S_z\rangle_j} \quad (8)$$

$$\frac{\delta_{ij}^{\text{para}}}{C_j} = F_i\frac{\langle S_z\rangle_j}{C_j} + B_0^2(G_i^1 + G_i^2) \quad (9)$$

Plots according to eqs 8 and 9 for $[Ln_2(L2)_3]^{6+}$ systematically show two straight lines for Ln = Ce−Eu and Ln = Tb−Yb with a break near the middle of the series (Figure 6). Two sets of F_i and $B_0^2(G_i^1 + G_i^2)$ are thus obtained by multilinear least-squares fits of eq 5 (Table 2), and the quality of the fittting processes measured by the *Wilcott* agreement factors (AF_i) [24] is satisfying for the observed protons ($i = 1-7$; $0.001 \le AF_i \le 0.08$, Table 2).

According to Table 2, the contact terms F_i significantly vary between the two series, but its eventual assignment to a structural change is prevented by the expected variation of B_0^2 along the lanthanide series.[25] The simultaneous consideration of the paramagnetic shifts of two different nuclei *i* and *k* in the same complex of a lanthanide *j* provides two equations similar to eq 5 which can be combined to remove the second-rank crystal-field parameter (eqs 10−12, two-nuclei method).[20,23,26]

$$\frac{\delta_{ij}^{\text{para}}}{\langle S_z\rangle_j} = B_{ik} + R_{ik}\frac{\delta_{kj}^{\text{para}}}{\langle S_z\rangle_j} \quad (10)$$

$$B_{iki} = F_i - F_k R_{ik} \quad (11)$$

$$R_{ik} = \frac{G_i^1 + G_i^2}{G_k^1 + G_k^2} \quad (12)$$

Application of the resulting two-nuclei crystal-field independent eq 10 for any aromatic pairs H*i*H*k* ($i \neq k$; $i, k = 1-6$) gives straight lines for plots of $\delta_{ij}^{\text{para}}/\langle S_z\rangle_j$ vs $\delta_{kj}^{\text{para}}/\langle S_z\rangle_j$ (Figure 7a), except for pairs involving H4 (Figure 7b) because both paramagnetic centers oppositely contribute to its pseudo-contact shifts (i.e., the $\theta_{H4}{}^m$ angles in the crystal structure of $[Tb_2(L2)_3]^{6+}$ are distributed on both sides of the magic angle $\theta = 54.7°$, Table S3, Supporting Information).[11,27] We conclude from the two-nuclei method that no significant structural variation occurs for $[Ln_2(L2)_3]^{6+}$ along the lanthanide series.

Since the two variables $\delta_{ij}^{\text{para}}/\langle S_z\rangle_j$ and $\delta_{kj}^{\text{para}}/\langle S_z\rangle_j$ in eq 10 form a homogeneous 2D Cartesian *x*,*y* frame, the best least-squares line is obtained by minimizing the sum of the squares of the perpendicular distances of the points from this line along the lanthanide series.[28] The slopes (R_{ik}) and the intercepts (B_{ik}) found in solution compare well with those calculated for the

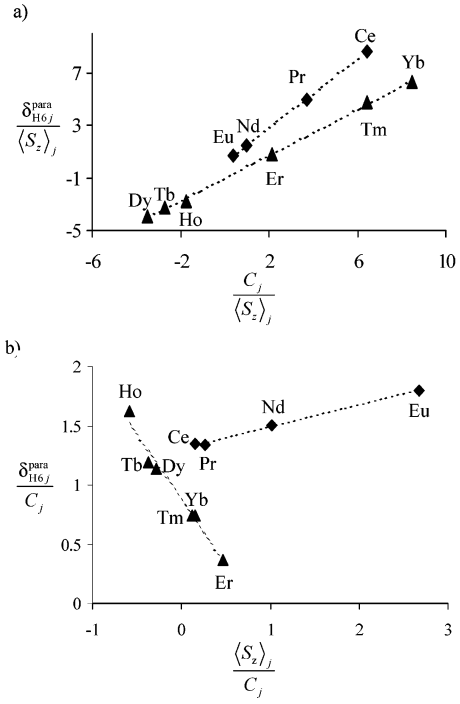

Figure 6. Plots of (a) $\delta_{ij}^{\text{para}}/\langle S_z\rangle_j$ vs $C_j/\langle S_z\rangle_j$ (eq 8) and (b) $\delta_{ij}^{\text{para}}/C_j$ vs $\langle S_z\rangle_j/C_j$ (eq 9) for H6 in $[Ln_2(L2)_3]^{6+}$ (CD_3CN, 298 K).

D_3-averaged crystal structure of $[Tb_2(L2)_3]^{6+}$ by using eqs 11 and 12 (Table S5, Supporting Information).[29] We conclude from the good correlation observed between the structural factors R_{ik}^{solution} and R_{ik}^{crystal} (Figure S5, Supporting Information) that (i) these supramolecular edifices are rather rigid and (ii) the triple-stranded helical structure exhibited in the solid state is maintained in solution along the complete lanthanide series. The break occurring near the middle of the lanthanide series with the one-nucleus method (eqs 8 and 9) can be thus safely assigned to a change in the crystal-field parameter B_0^2 amplified by the abrupt increase of C_j in going from Ln = Ce−Eu to Ln = Tb−Yb.[20,21,30,31] Linear least-squares fits of $B_0^2(G_i^1 + G_i^2)$ measured in solution (Table 2) vs $(G_i^{1\text{crystal}} + G_i^{2\text{crystal}})$ calculated for $[Tb_2(L2)_3]^{6+}$ in the solid state (Table S3, Supporting Information)[11] give $B_0^2(\text{Ln} = \text{Ce}-\text{Eu}) = -69(2)$ ppm Å^3 and $B_0^2(\text{Ln} = \text{Tb}-\text{Yb}) = -44(3)$ ppm Å^3. The ratio $B_0^2(\text{Ln} = \text{Ce}-\text{Eu})/B_0^2(\text{Ln} = \text{Tb}-\text{Yb}) = 1.58(2)$ found for $[Ln_2(L2)_3]^{6+}$ matches 1.6(2) reported for the heterobimetallic d−f triple-stranded helicate $[LnCo(L7)_3]^{6+}$ [4d] and 1.5(1) for [Ln(2,6-dipicolinate)$_3$]$^{3-}$.[32]

Speciation and Formation Constants of the Heterobimetallic Helicates $[(Ln^1)(Ln^2)(L2)_3]^{6+}$ (Ln^1, Ln^2 = La, Nd, Sm, Eu, Yb, Lu, Y). Since (i) a single D_3-symmetrical structure has been unambiguously established for $[Ln_2(L2)_3]^{6+}$ along the complete lanthanide series and (ii) the formation constants

(24) Wilcott, M. R.; Lenkinski, R. E.; Davis, R. E. *J. Am. Chem. Soc.* **1972**, *94*, 1742.
(25) (a) Freeman, A. J.; Watson, R. E. *Phys. Rev. B.* **1962**, *127*, 2058. (b) Hopkins, T. A.; Bolender, J. P.; Metcalf, D. H.; Richardson, F. S. *Inorg. Chem.* **1996**, *35*, 5356. (c) (b) Görller-Walrand, C.; Binnemans, K. In *Handbook on the Physics and Chemistry of Rare Earths*; Gschneidner, K. A., Jr., Eyring, L., Eds.; North-Holland Publishing Company, Amsterdam, 1996; Vol. 23, pp 121−283. (d) Hopkins, T. A.; Metcalf, D. H.; Richardson, F. S. *Inorg. Chem.* **1998**, *37*, 1401. (e) Ishikawa, N. *J. Phys. Chem. A* **2003**, *107*, 5831.
(26) (a) Reuben, J. *J. Magn. Reson.* **1982**, *50*, 233. (b) Spiliadis, S.; Pinkerton, A. A. *J. Chem. Soc., Dalton Trans.* **1982**, 1815. (c) Ren, J.; Sherry, A. D. *J. Magn. Reson.* **1996**, *B111*, 178. (d) Platas, C.; Avecilla, F.; de Blas, A.; Geraldes, C. F. G. C.; Rodriguez-Blas, T.; Adams, H.; Mahia, J. *Inorg. Chem.* **1999**, *38*, 3190.
(27) Rigault, S.; Piguet, C.; Bünzli, J.-C. G. *J. Chem. Soc., Dalton Trans.* **2000**, 2045.
(28) This problem is solved by using a so-called *Lagrangian* multiplier and a software for symbolic computation as previously described in ref 32 (see Experimental Section).
(29) For each proton H*i*, the geometrical factors $G_i^1 = (3\cos^2\theta_i^1 - 1)/(r_i^1)^3$ and $G_i^2 = (3\cos^2\theta_i^2 - 1)/(r_i^2)^3$ are calculated by using θ_i and r_i taken from the crystal structure of $[Tb_2(L2)_3]^{6+}$.[11] The average D_3-symmetry is obtained by averaging the six symmetrically related values of G_i^1, respectively G_i^2, for each proton. F_i are taken from Table 2.
(30) Ouali, N.; Rivera, J.-P.; Chapon, D.; Delangle, P.; Piguet, C. *Inorg. Chem.* **2004**, *43*, 1517.
(31) Ouali, N.; Rivera, J.-P.; Morgantini, P.-Y.; Weber, J.; Piguet, C. *Dalton Trans.* **2003**, 1251.

Table 2. Computed Values for Contact (F_i) and Pseudo-Contact ($S_i = B_0^2(G_i^1 + G_i^2)$) Terms and Agreement Factors (AF_i) for Aromatic and Methylene Protons in Complexes $[Ln_2(L2)_3]^{6+}$ (CD_3CN, 298 K)[a]

compd	H1	H2	H3	H4	H5	H6	H7
			Ln = Ce−Eu				
F_i	−0.18(1)	−0.10(1)	−0.23(1)	−0.100(6)	0.025(3)	0.19(2)	0.038(1)
S_i	−0.148(9)	−0.19(1)	−0.237(9)	0.003(4)	0.076(2)	1.29(1)	0.104(1)
AF_i[b]	0.009	0.009	0.007	0.005	0.002	0.01	0.001
			Ln = Tb−Yb				
F_i	0.06(3)	0.15(3)	0.02(3)	−0.09(1)	−0.05(1)	−1.0(1)	−0.072(9)
S_i	−0.070(9)	−0.10(1)	−0.102(9)	0.029(4)	0.065(6)	0.85(4)	0.063(9)
AF_i[b]	0.07	0.07	0.05	0.05	0.08	0.05	0.06

[a] F_i and S_i are obtained by multilinear least-squares fits of δ_{ij}^{para} vs $\langle S_z\rangle_j$ and C_j (eq 5), and Sm(III) is not considered because of its faint paramagnetism.

[b] Calculated according to $AF_i = \sqrt{\frac{\sum_j(\delta_{ij}^{obs} - \delta_{ij}^{calc})^2}{\sum_j(\delta_{ij}^{obs})^2}}$.[24]

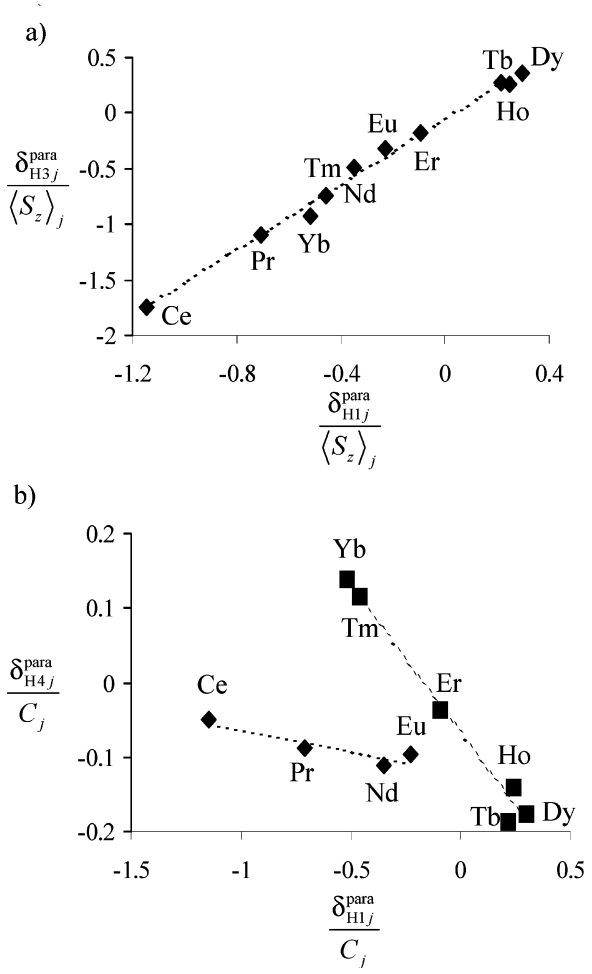

Figure 7. Crystal-field independent plots of $\delta_{ij}^{para}/\langle S_z\rangle_j$ vs $\delta_{kj}^{para}/S_z\rangle_j$ (eq 10) for (a) the H1−H3 pair and (b) the H1−H4 pair (CD_3CN, 298 K).

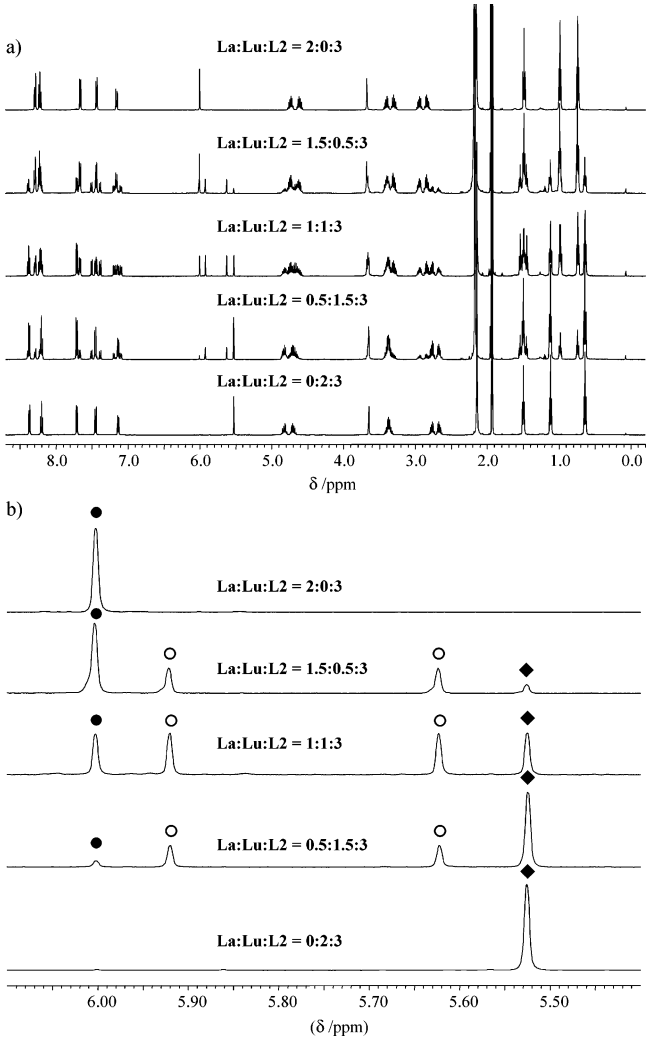

Figure 8. ^1H NMR spectra of $[La_xLu_{2-x}(L2)_3]^{6+}$ for different La/Lu/L2 ratios. (a) Complete spectra and (b) magnification of the signals of H6 with ● = $[La_2(L2)_3]^{6+}$, ○ = $[LaLu(L2)_3]^{6+}$, and ◆ = $[Lu_2(L2)_3]^{6+}$ (CD_3CN, 298 K).

$\log(\beta_{23}^{bi,LnLn})$ (Table 1) are large enough to ensure that $[Ln_2(L2)_3]^{6+}$ is quantitatively formed under stoichiometric conditions during the NMR experiments (>95% of the ligand speciation for Ln/L2 = 0.67, $[L2]_{tot} = 10^{-2}$ M, CD_3CN), we can reasonably assume that the reaction of L2 with two different trivalent lanthanides, Ln^1 and Ln^2, exclusively produces a mixture of the homobimetallic helicates $[(Ln^1)_2(L2)_3]^{6+}$, $[(Ln^2)_2(L2)_3]^{6+}$ together with the heterobimetallic complexes $[(Ln^1)(Ln^2)(L2)_3]^{6+}$. For all investigated pairs (Ln1, Ln2 = La, Nd, Sm, Eu, Yb, Lu, Y, Table S6, Supporting Information), the ^1H NMR spectra indeed confirms the exclusive formation of the three expected species (further termed $(Ln^1)_2$, $(Ln^2)_2$ and $(Ln^1)(Ln^2)$ for the sake of simplicity) in various amounts depending on the $Ln^1/Ln^2/L2$ ratios (Figure 8 and Table S6, Supporting Information).

For lanthanide pairs containing at least one paramagnetic metal, a reliable characterization of the heterobimetallic helicate is difficult and the ^1H NMR spectra of the C_3-symmetrical (Ln^p)-

Table 3. Formation Constants $\log(\beta_{23}^{bi,Ln^1Ln^2})$ Obtained by ^1H NMR for the Complexes $[(Ln^1)_x(Ln^2)_{2-x}(L2)_3]^{6+}$ (Ln^1, Ln^2 = La, Nd, Sm, Eu, Yb, Lu, Y; $x = 0-2$, CD_3CN, 298 K)[a]

complex	$\log(\beta_{23}^{bi,Ln^1Ln^2})$	complex	$\log(\beta_{23}^{bi,Ln^1Ln^2})$
$[La_2(L2)_3]^{6+}$	25.1(1)	$[SmLu(L2)_3]^{6+}$	25.8(1)
$[LaLu(L2)_3]^{6+}$	25.5(1)	$[SmYb(L2)_3]^{6+}$	25.9(1)
$[LaYb(L2)_3]^{6+}$	25.5(1)	$[SmY(L2)_3]^{6+}$	26.0(1)
$[LaY(L2)_3]^{6+}$	25.7(1)	$[SmEu(L2)_3]^{6+}$	26.1(1)
$[LaEu(L2)_3]^{6+}$	25.8(1)	$[Eu_2(L2)_3]^{6+}$	25.9(1)
$[LaSm(L2)_3]^{6+}$	25.7(1)	$[EuLu(L2)_3]^{6+}$	25.9(1)
$[LaNd(L2)_3]^{6+}$	25.5(1)	$[EuYb(L2)_3]^{6+}$	26.0(1)
$[Nd_2(L2)_3]^{6+}$	25.3(1)	$[EuY(L2)_3]^{6+}$	26.1(1)
$[NdLu(L2)_3]^{6+}$	25.6(1)	$[Y_2(L2)_3]^{6+}$	25.8(1)
$[NdYb(L2)_3]^{6+}$	25.7(1)	$[YLu(L2)_3]^{6+}$	25.9(1)
$[NdY(L2)_3]^{6+}$	25.8(1)	$[YYb(L2)_3]^{6+}$	25.9(1)
$[NdEu(L2)_3]^{6+}$	25.9(1)	$[Yb_2(L2)_3]^{6+}$	25.5(1)
$[NdSm(L2)_3]^{6+}$	25.8(1)	$[YbLu(L2)_3]^{6+}$	25.7(1)
$[Sm_2(L2)_3]^{6+}$	25.7(1)	$[Lu_2(L2)_3]^{6+}$	25.3(1)

(Ln^q) helicates have been predicted by using eq 13 (i.e., an extension of eq 5 adapted to heterobimetallic complexes),[13] together with (i) the crystal-field parameters B_0^2 previously determined for the homobimetallic complexes in solution, and (ii) G_i^1 and G_i^2 taken from the crystal structure of $[Tb_2(L2)_3]^{6+}$ (Table S3, Supporting Information).[11]

$$\delta_{ij}^{para} = F_i^{p,q}\langle S_z\rangle_{p,q} + G_i^1 B_0^{\,2p} C_p + G_i^2 B_0^{\,2q} C_q \qquad (13)$$

The calculated spectra closely match the experimental data (Figures S6 and S7, Supporting Information), thus leading to a reliable assignment of heterobimetallic helicates for each investigated pair (Table S7, Supporting Information). Taking the $\log(\beta_{23}^{bi,LnLn})$ values determined by spectrophotometry for the Ln_2 helicates as initial estimations (Table 1), the formation constants for each homo- ($\log(\beta_{23}^{bi,LnLn})$, equilibrium 2) and heterobimetallic helicate ($\log(\beta_{23}^{bi,Ln^1Ln^2})$, equilibrium 14) observed in solution can be adjusted with the program MINEQL^{+}[33] by fitting their relative experimental proportions determined by ^1H NMR for different Ln^1/Ln^2 ratios (Table S6, Supporting Information).[13] Within experimental error, identical $\log(\beta_{23}^{bi,LnLn})$ are obtained for the same homobimetallic complexes contributing in different pairs (e.g., $\log(\beta_{23}^{bi,LnLn})$ determined for the La/Y, La/Sm, or La/Lu pairs), and the average values (Table 3) are in very good agreement with those obtained by spectrophotometry (Table 1)

$$[Ln^1]^{3+} + [Ln^2]^{3+} + 3L2 \rightleftharpoons [(Ln^1)(Ln^2)(L2)_3]^{6+}\ \log(\beta_{23}^{bi,Ln^1Ln^2}) \qquad (14)$$

Modeling the Thermodynamic Assembly of Homo- and Heterobimetallic Helicates $[(Ln^1)_x(Ln^2)_{2-x}(L2)_3]^{6+}$ (Ln^1, Ln^2 = La, Nd, Sm, Eu, Yb, Lu, Y; $x = 0-2$). The thermodynamic *site-binding* model described in Figure 1[13b] has been adapted for the treatment of the thermodynamic data obtained for $[(Ln^1)_x(Ln^2)_{2-x}(L2)_3]^{6+}$ (Figure 9). Each bimetallic helicate is thus made up of a preassembled receptor $[L2]_3$ in which the two equivalent N_6O_3 sites are available for the coordination of Ln(III). According to Figure 9, the total free energy for the formation of each $(Ln^1)_x(Ln^2)_{2-x}$ helicate is given by eq 15, whereby s is the degeneracy of the microscopic state.[13b,14] In the latter equation, the free energy cost associated with the preorganization of the three ligands in a triple-helical fashion to produce the box is neglected because it similarly affects the formation of any C_3-symmetrical lanthanide complexes matching

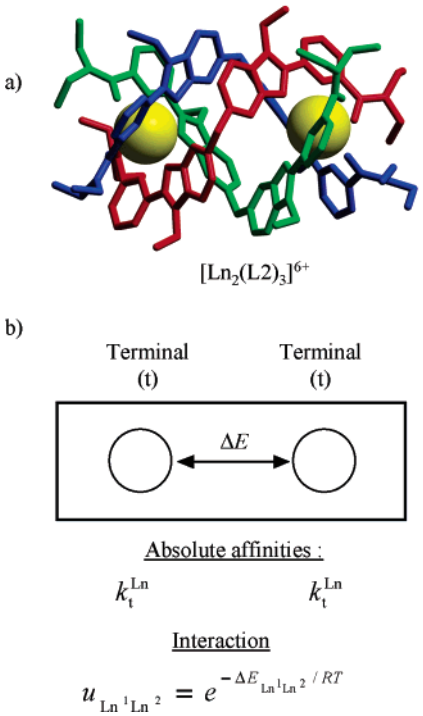

Figure 9. (a) Crystal and solution structure of $[Ln_2(L2)_3]^{6+}$ and (b) associated thermodynamic *site-binding* model.

the *site-binding* model shown in Figure 9. This contribution thus corresponds to a fixed translation of the zero-level of the free energy scale which is arbitrarily set to zero.

$$\Delta G_{tot}([Ln_x^{\,1}Ln_{2-x}^{\,2}]) = -xRT\ln(k_t^{Ln^1}) - (2-x)RT\ln(k_t^{Ln^2}) + \Delta E_{Ln^1Ln^2} - RT\ln(s) = -RT\ln(\beta_{23}^{bi,Ln^1Ln^2}) \qquad (15)$$

For the D_3-symmetrical homobimetallic helicates $(Ln^1)_2$ and $(Ln^1)_2$, the macroscopic constants $\beta_{23}^{bi,LnLn}$ (Table 3) coincide with their microscopic description (i.e., $s = 1$), and application of eq 15 provides eqs 16 and 17, respectively, assuming that $u_{LnLn} = e^{-(\Delta E_{LnLn}/RT)}$. For the heterobimetallic helicates (Ln^1)-(Ln^2), the degeneracy $s = 2$ and eq 18 results. A similar treatment leads to eqs 19 and 20 for the unsaturated intermediates $[(Ln^1)(L2)_3]^{3+}$ and $[(Ln^2)(L2)_3]^{3+}$, respectively.

$$\beta_{23}^{bi,Ln^1Ln^1} = (k_t^{Ln^1})^2 \cdot u_{Ln^1Ln^1} \qquad (16)$$

$$\beta_{23}^{bi,Ln^2Ln^2} = (k_t^{Ln^2})^2 \cdot u_{Ln^2Ln^2} \qquad (17)$$

$$\beta_{23}^{bi,Ln^1Ln^2} = 2(k_t^{Ln^1})(k_t^{Ln^2}) \cdot u_{Ln^1Ln^2} \qquad (18)$$

$$\beta_{13}^{bi,Ln^1} = 2(k_t^{Ln^1}) \qquad (19)$$

$$\beta_{13}^{bi,Ln^2} = 2(k_t^{Ln^2}) \qquad (20)$$

Since eqs 16−20 are independent, the five parameters $k_t^{Ln^1}$, $k_t^{Ln^2}$, $u_{Ln^1Ln^1}$, $u_{Ln^2Ln^2}$, and $u_{Ln^1Ln^2}$ can be calculated. However, such a statistical description of error-containing experimental constants requires an overdetermined system for extracting physically meaningful parameters, and the simplification $u_{Ln^1Ln^1} = u_{Ln^2Ln^2} = u_{Ln^1Ln^2} = u$ has been used for limiting the number

Table 4. Absolute Affinities for the Terminal N_6O_3 ($\log(k_t^{Ln})$) and for the Central N_9 ($\log(k_c^{Ln})$) Metallic Sites in the Triple-Stranded Helicates $[Ln_2(L2)_3]^{6+}$ and $[Ln_3(L5)_3]^{9+}$ Obtained with Nonlinear Least-Squares Fits

Ln	r_{Ln}/Å[a]	$\log(k_t^{Ln})$[b]	$\log(k_t^{Ln})$[c]	$\log(k_c^{Ln})$[c]
La	1.216	16.9(4)	16.8(4)	18.2(7)
Nd	1.163	17.7(4)	17.6(4)	19.6(7)
Sm	1.132	17.4(4)	17.1(4)	17.9(7)
Eu	1.120	18.2(4)	18.1(4)	19.5(7)
Y	1.075	17.2(4)	17.1(4)	17.1(7)
Yb	1.042	17.1(4)	16.4(4)	16.1(7)
Lu	1.032	17.0(4)	17.3(4)	18.0(7)

[a] r_{Ln} = nine-coordinate ionic radius.[18] [b] Computed by using the data of the bimetallic helicates $[(Ln^1)_x(Ln^2)_{2-x}(L2)_3]^{6+}$ ($x = 0-2$ and eqs 16−20). [c] Computed by using the global set of data obtained for the bimetallic helicates $[(Ln^1)_x(Ln^2)_{2-x}(L2)_3]^{6+}$ ($x = 0-2$, eqs 16−20) and for the trimetallic helicates $[(Ln^1)_x(Ln^2)_{3-x}(L5)_3]^{9+}$ ($x = 0-3$, eqs 31−36).

of parameters. This assumption is justified by the average experimental exchange constant $K_{exch} = 4.0(3)$ found for equilibrium 21 (Table S6, Supporting Information), which does not vary from its statistical value $K_{exch} = 4$ calculated with eq 22 (obtained by applying eqs 16−18 to equilibrium 21).[34]

$$[(Ln^1)_2(L2)_3]^{6+} + [(Ln^2)_2(L2)_3]^{6+} \rightleftharpoons 2[(Ln^1)(Ln^2)(L2)_3]^{6+} K_{exch} \quad (21)$$

$$K_{exch} = 4(u_{Ln^1Ln^2})^2/(u_{Ln^1Ln^1} \cdot u_{Ln^2Ln^2}) \quad (22)$$

For each Ln^1/Ln^2 pair, we have therefore considered five experimental macroscopic stability constants (eqs 16−20) for extracting the three parameters $k_t^{Ln^1}$, $k_t^{Ln^2}$, u by using nonlinear least-squares techniques (Table 4 and Table S8, Supporting Information).[35] Good agreement is systematically observed for similar parameters extracted from the analyses of different pairs containing a common lanthanide, and the recalculated formation constants $\log(\beta_{13}^{bi,calc})$ and $\log(\beta_{23}^{bi,calc})$ fairly match the experimental data, which supports the reliability of the fitting process (maximum relative discrepancy: 4%, Table 1).

Interestingly, the concave bowl-shape curve found for $\log(\beta_{23}^{bi,LnLn})$ vs the inverse of the ionic radii of nine-coordinate Ln(III) (Figure 10a) is reminiscent of a closely related trend observed for the absolute affinities $\log(k_t^{Ln})$ (Figure 10b), while the free energy interaction parameters ΔE are randomly distributed around the average value $\bar{\Delta}\bar{E} = 51(7)$ kJ mol^{-1}, and they do not depend on the nature of the selected pairs (Figure 10c and Table S8, Supporting Information).

The rather large interaction parameter ΔE points to strong negative cooperativity, and it can be compared with the electrostatic work required for complexing two Ln(III) considered as simple triply charged dots separated by $R_{Ln-Ln} = 9.06$ Å (taken from the crystal structures of $[Tb_2(L2)_3]^{6+}$).[11] Equation 23 holds in which q stands for the electrostatic charge (1.602×10^{-19} C), ϵ_0 is the vacuum permittivity constant (8.84×10^{-12} C^2 N^{-1} m^{-2}), and ϵ_{rel} is the relative dielectric constant of the medium separating the trivalent point charges during the complexation process.[4d,36]

$$W = \frac{9q^2}{4\pi\epsilon_0}\int_{R_{LnLn}}^{\infty} \frac{1}{\epsilon_{rel} r^2} dr \quad (23)$$

When the Ln^{3+} cations are well-separated in solution, $\epsilon_{rel} = \epsilon_{acetonitrile} = 36.2$,[37] and this value slightly reduces to $\epsilon_{rel} \approx 30$ in the triple-stranded helicate.[4d,36] We have thus used an average constant value of $\epsilon_{rel} \approx 30$ for calculating $W \approx 48$ kJ mol^{-1} with eq 23, a value which matches the average interaction parameter $\bar{\Delta}\bar{E} = 51(7)$ kJ mol^{-1} in $[Ln_2(L2)_3]^{6+}$. This suggests that the origin of the strong repulsive intermetallic interaction is mainly electrostatic.

Repetitive Statistical Binding in the Self-Assembly of Triple-Stranded Helicates. In his seminal contribution, *Ercolani* demonstrates that tests for repetitive statistical binding (i.e., the successive filling of coordination sites with a fixed interaction parameter ΔE) in self-assembled architectures require a careful separation of the intermolecular processes which are responsible for the organization of the ligands with a minimum of metal ions to produce a "receptor" and the subsequent intramolecular complexation processes leading to multimetallic assemblies.[15] In *Ercolani*'s model, the overall self-assembly of a triple-stranded helicate $[Ln_m(Li)_3]^{3m+}$ containing $N = m + 3$ components is thus described by equilibrium 24, while the associated microscopic constant K_{m3} is given by eq 25.[15]

$$mLn^{3+} + 3Li \rightleftharpoons [Ln_m(Li)_3]^{3m+} K_{m3} \quad (24)$$

$$K_{m3} = \sigma_{sa} \cdot K_{inter}^{N-1} \cdot K_{intra}^{B-N+1} \quad (25)$$

$\sigma_{sa} = \sigma_{Ligand}^3 \cdot \sigma_{Metal}^m/\sigma_{Complex}$ is the symmetry factor of the self-assembly equilibrium 24 ($\sigma_{Metal} = 1$, $\sigma_{Ligand} = 2$ and $\sigma_{Complex}$-(*FAC*-$[Ln(Li)_3]^{3+}$) = 3, $\sigma_{Complex}$(*MER*-$[Ln(Li)_3]^{3+}$) = 1, $\sigma_{Complex}$-($[Ln_2(Li)_3]^{6+}$) = $\sigma_{Complex}$($[Ln_3(Li)_3]^{9+}$) = 6),[38] K_{inter} is the microscopic intermolecular equilibrium constant associated with the formation of $[Ln(Li)_3]^{3+}$, K_{intra} is the microscopic (statistically corrected) intramolecular constant associated with the subsequent complexation of Ln(III) to $[Ln(Li)_3]^{3+}$, and $B = 3m$ is the number of connections joining the components in $[Ln_m(Li)_3]^{3m+}$.[15] The two macroscopic constants $\beta_{13}^{bi,Ln}$ (eq 1) and $\beta_{23}^{bi,LnLn}$ (eq 2) for the formation of $[Ln(L2)_3]^{3+}$ and $[Ln_2(L2)_3]^{6+}$can be expressed with eq 25 to give eqs 26 and 27, respectively.

$$\beta_{13}^{bi,Ln} = 2(\sigma_{sa}^{facial} + \sigma_{sa}^{meridional})(K_{inter}^{Ln})^3 \quad (26)$$

$$\beta_{23}^{bi,LnLn} = 2\sigma_{sa}^{bi}(K_{inter}^{Ln})^4(K_{intra}^{Ln})^2 \quad (27)$$

The additional factor 2 multiplying the right-hand sides of eqs 26 and 27 results from the formation of chiral edifices from achiral ligands and metal ions.[15] The mathematical resolution of eqs 26 and 27 with the symmetry factors $\sigma_{sa}^{facial} = 8/3$, $\sigma_{sa}^{meridional} = 8$ and $\sigma_{sa}^{bi} = 4/3$,[15,38] and $\beta_{13}^{bi,Ln}$ and $\beta_{23}^{bi,LnLn}$ taken from Table 1 gives K_{inter}^{Ln} and K_{intra}^{Ln} collected in Table S9 (Supporting Information).

(32) Ouali, N.; Bocquet, B.; Rigault, S.; Morgantini, P.-Y.; Weber, J.; Piguet, C. *Inorg. Chem.* **2002**, *41*, 1436.
(33) Schecher, W. *MINEQL*$^+$, version 2.1; MD Environmental Research Software; Edgewater, NJ, 1991.
(34) We assume that, since $u_{Ln^1Ln^2}^2/(u_{Ln^1Ln^1} \cdot u_{Ln^2Ln^2}) = 1$ for all investigated pairs, $u_{Ln^1Ln^1} = u_{Ln^2Ln^2} = u_{Ln^1Ln^2} = u$.
(35) Borkovec, M. *FITMIX*, a programm for the nonlinear fit of multimetallic complexation in polymetallic complexes.
(36) (a) Serr, B. R.; Andersen, K. A.; Elliott C. M.; Anderson O. P. *Inorg. Chem.* **1988**, *27*, 4499. (b) Cantuel, M.; Bernardinelli, G.; Muller, G.; Riehl, J. P.; Piguet, C. *Inorg. Chem.* **2004**, *43*, 1840−1849.
(37) Geary, W. J. *Coord. Chem. Rev.* **1971**, *7*, 81.
(38) (a) See note 10 in ref 15. (b) Lowry, T. H.; Richardson, K. S. *Mechanism and Theory in Organic Chemistry*, 3rd ed.; Harper &Row: New York, 1987; pp 175−177.

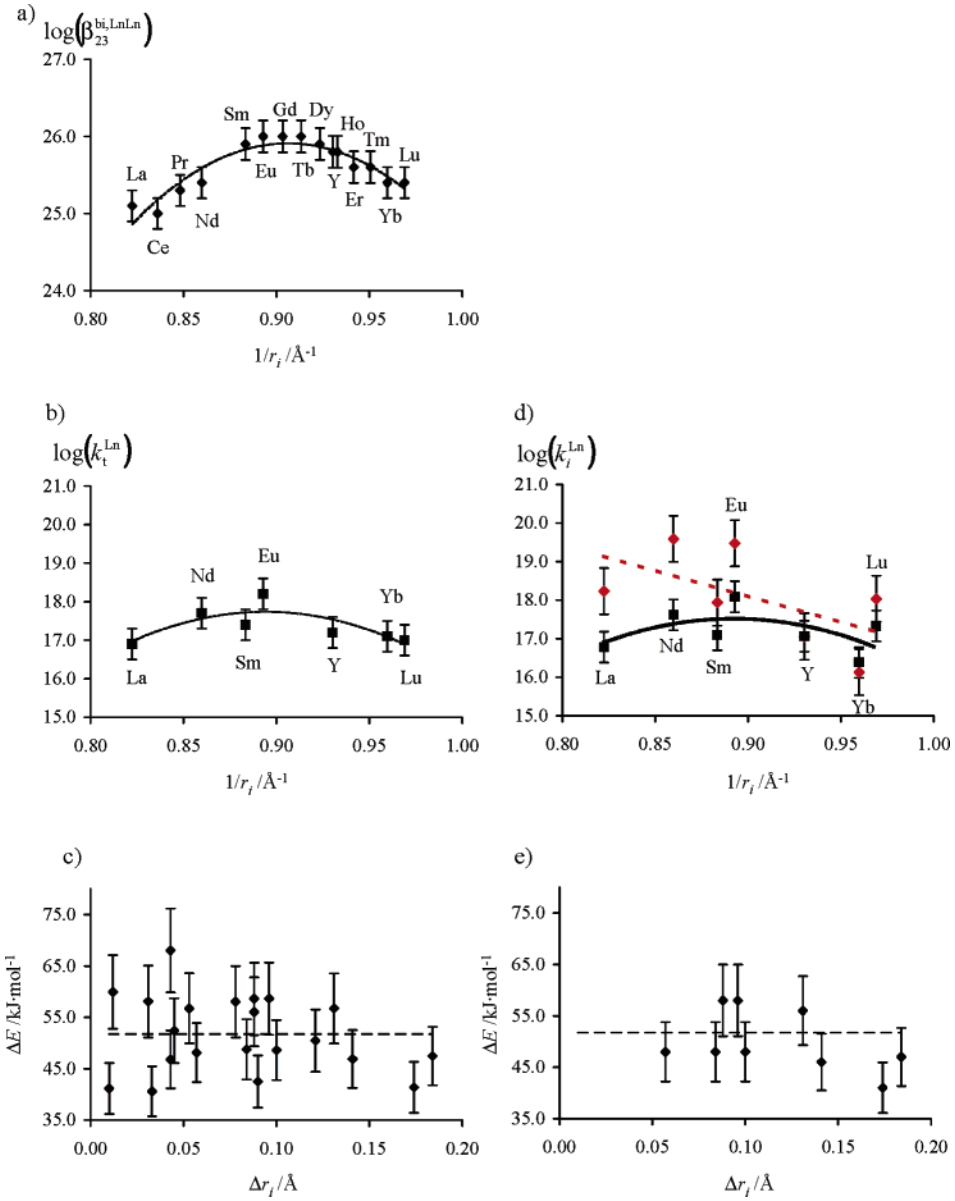

Figure 10. (a) Experimental macroscopic formation constants ($\log(\beta_{23}^{bi,LnLn})$, Table 1). (b) Computed absolute affinities for the terminal sites ($\log(k_t^{Ln})$) and (c) intermetallic interaction parameters (ΔE) in the triple-stranded bimetallic helicates $[Ln_2(L2)_3]^{6+}$ as a function of the inverse or the difference of nine-coordinate ionic radii ($\Delta r_i = |r_{Ln}^1 - r_{Ln}^2|$).[18] (d) Related computed absolute affinities for the terminal ($\log(k_t^{Ln})$; ■) and central ($\log(k_c^{Ln})$;◆) sites and (e) intermetallic interaction parameters (ΔE) in the triple-stranded trimetallic $[Ln_3(L5)_3]^{9+}$ helicates. The trend lines are only guides for the eyes.

Considering the rather similar affinities of the N_6O_3 site in $[Ln(L6)_3]^{3+}$ and of the N_9 site in $[Ln(L8)_3]^{3+}$,[19] we can reasonably approximate that each site in the trimetallic $[Ln_3(L5)_3]^{9+}$ displays the same affinity as that found for the terminal sites in $[Ln_2(L2)_3]^{6+}$. The statistical formation constants for the trimetallic helicates $[Ln_3(L5)_3]^{9+}$ (equilibrium 28, $\log(\beta_{33}^{tri,stat})$) can be thus estimated with eq 29 ($\sigma_{sa}^{tri} = 4/3$).[15,38]

$$3Ln^{3+} + 3L5 \rightleftharpoons [Ln_3(L5)_3]^{9+} \quad \log(\beta_{33}^{tri,stat}) \qquad (28)$$

$$\beta_{33}^{tri,stat} = 2\sigma_{sa}^{tri}(K_{inter}^{Ln})^5(K_{intra}^{Ln})^4 \qquad (29)$$

The predicted statistical constants $\log(\beta_{33}^{tri,stat})$ closely match the experimental data (Table S9, Supporting Information),[13] and we eventually conclude that the assembly process leading to the trimetallic helicates $[Ln_3(L5)_3]^{9+}$ evidences repetitive statistical binding (i.e., the absolute affinities of each site for Ln(III) and the intermetallic repulsions are similar in the homologous series of mono-, bi- and trimetallic helicates).[15] This model can be further refined by taking into account that $[Ln(L2)_3]^{3+}$ exists in solution as the single facial isomer (vide infra). The removal of the contribution of the meridional isomer transforms eq 26 into eq 30, and a new slightly modified set of K_{inter}^{Ln} and K_{intra}^{Ln} is obtained (Table S9, Supporting Information).

$$\beta_{13}^{bi,Ln} = 2\sigma_{sa}^{facial}(K_{inter}^{Ln})^3 \qquad (30)$$

The use of eq 29 then provides $\beta_{33}^{tri,stat}$ which are approximately 1 order of magnitude smaller than $\beta_{33}^{tri,LnLnLn}$, in complete agreement with the larger absolute affinity (i.e., 1 order of magnitude) observed for the central N_9 site ($\log(k_c^{Ln}) > \log(k_t^{Ln})$, Table 4). The latter cannot be accounted for by eq 29, because $[Ln_3(L5)_3]^{9+}$ is considered as being made up of three successive terminal sites.

A Global Approach for the Thermodynamic Programming of Multimetallic Helicates. Since the assemblies of $[Ln(L2)_3]^{3+}$, $[Ln_2(L2)_3]^{6+}$, and $[Ln_3(L5)_3]^{9+}$ display repetitive statistical binding, (i) the terminal N_6O_3 sites in $[Ln_2(L2)_3]^{6+}$ (Figure 9) and in $[Ln_3(L5)_3]^{9+}$ (Figure 1) are characterized by the same absolute affinity constant k_t^{Ln}, (ii) the free energy required for preorganizing $[L2]_3$ and $[L5]_3$ are similar and can be set to zero, and (iii) the intermetallic electrostatic interaction ΔE calculated for the bimetallic helicates also holds in the trimetallic analogues (i.e., a Ln···Ln separation of ≈ 9.1 Å is maintained in both types of complexes).[11,13] Therefore, eqs 16−20, associated with the assembly of $[Ln_2(L2)_3]^{6+}$, can be combined with eqs 31−36 adapted to that of the trimetallic helicates $[Ln_3(L5)_3]^{9+}$,[13b] and global nonlinear least-squares fits[35] for the nine different Ln^1/Ln^2 pairs provide five parameters $k_t^{Ln^1}$, $k_t^{Ln^2}$, $k_c^{Ln^1}$, $k_c^{Ln^2}$, and u from the simultaneous consideration of 9−11 independent equations (again assuming that $u_{Ln^1Ln^1} \approx u_{Ln^2Ln^2} \approx u_{Ln^1Ln^2} = u$ and that repulsion between non-neighboring metals being negligible). The final values of $\log(k_t^{Ln})$ and $\log(k_c^{Ln})$ are summarized in Table 4, and the free energy interaction parameters ΔE are randomly distributed around the average value $\bar{\Delta E} = 51(6)$ kJ mol^{-1} (Figure 10e and Table S10, Supporting Information).

$$\beta_{33}^{tri,Ln^1Ln^1Ln^1} = (k_t^{Ln^1})^2(k_c^{Ln^1})(u_{Ln^1Ln^1})^2 \quad (31)$$

$$\beta_{33}^{tri,Ln^1Ln^1Ln^2} = 2(k_t^{Ln^1})(k_c^{Ln^1})(k_t^{Ln^2})u_{Ln^1Ln^1}u_{Ln^1Ln^2} \quad (32)$$

$$\beta_{33}^{tri,Ln^1Ln^2Ln^1} = (k_t^{Ln^1})^2(k_c^{Ln^2})(u_{Ln^1Ln^2})^2 \quad (33)$$

$$\beta_{33}^{tri,Ln^1Ln^2Ln^2} = 2(k_t^{Ln^1})(k_c^{Ln^2})(k_t^{Ln^2})u_{Ln^1Ln^2}u_{Ln^2Ln^2} \quad (34)$$

$$\beta_{33}^{tri,Ln^2Ln^1Ln^2} = (k_t^{Ln^2})^2(k_c^{Ln^1})(u_{Ln^1Ln^2})^2 \quad (35)$$

$$\beta_{33}^{tri,Ln^2Ln^2Ln^2} = (k_t^{Ln^2})^2(k_c^{Ln^2})(u_{Ln^2Ln^2})^2 \quad (36)$$

The values of $\log(k_t^{Ln})$ and ΔE found by the global analysis closely match those previously found for the same treatment applied to the bimetallic helicates in agreement with a statistical thermodynamic model, which predicts that the magnitudes of the free energy of complexation of the terminal N_6O_3 site ($-103(4) \le \Delta G_t^\circ = -RT\ln(k_t^{Ln}) \le -96(4)$ kJ mol^{-1}) and of the intermetallic repulsion parameter ΔE are roughly invariant in a homologous series of multimetallic helicates (Table 4). Obviously, the concave trend previously noted for $\log(k_t^{Ln})$ is maintained (Figure 10d), while $\log(k_c^{Ln})$ exhibits a monotonic decrease when going from large (Ln = La) to small (Ln = Lu) lanthanides (Figure 10d). The latter trend was previously reported for the monometallic complexes $[Ln(L8)_3]^{3+}$ (a structural model of the central site in $[Ln_3(L5)_3]^{9+}$).[39] We also note that the absolute affinities of the central N_9 site (k_c^{Ln}) are approximately 1 order of magnitude larger than those for the terminal N_6O_3 site (k_t^{Ln}, i.e., a stabilization of ca. 5−10 kJ mol^{-1}), a trend which also agrees with the one reported for the monometallic complexes $[Ln(L8)_3]^{3+}$ and $[Ln(L6)_3]^{3+}$.[19] Finally, the comparison between the experimental and the calculated formation constants of the unsaturated complexes $[Ln(L2)_3]^{3+}$ ($\log(\beta_{13}^{bi,Ln})$, eqs 19 and 20) is satisfying (Table S11, Supporting Information), while the calculated constants for the unsaturated intermediate $[Ln_2(L5)_3]^{6+}$ ($\log(\beta_{23}^{tri,calc})$, eqs 37 and 38) are approximately 10 orders of magnitude larger than the experimental data (Table S11, Supporting Information).

Scheme 2. Postulated Structure of $[Ln_2(L5)_3]^{6+}$ in Acetonitrile

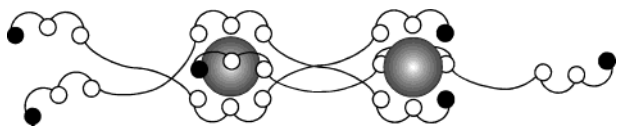

$$\beta_{23}^{tri,Ln^1Ln^1} = (k_t^{Ln^1})^2 + 2(k_t^{Ln^1})(k_c^{Ln^1})u_{Ln^1Ln^1} \quad (37)$$

$$\beta_{23}^{tri,Ln^2Ln^2} = (k_t^{Ln^2})^2 + 2(k_t^{Ln^2})(k_c^{Ln^2})u_{Ln^2Ln^2} \quad (38)$$

Separation of the macroconstants ($\log(\beta_{23}^{tri,LnLn})$) into the two microconstants described by eq 37 or eq 38 shows that the complex in which the central site is not occupied (microconstant $= (k_t^{Ln})^2 = 10^{33-36}$) is predicted to be more stable than the one in which the two metal ions occupy neighboring sites (microconstant $= 2(k_t^{Ln})(k_c^{Ln})u = 10^{25-28}$). As a consequence, the latter complex is negligible in our model. However, the derived microconstants compare well with the experimental macroconstants $\beta_{23}^{tri,LnLn} = 10^{25-26}$ (Table S11, Supporting Information), which strongly suggests that (i) the unsaturated complex cannot accept two Ln(III) in its terminal sites in $[Ln_2(L5)_3]^{6+}$ and (ii) the *site-binding* model shown in Figure 1 is not adequate for these complexes. Since nothing is known about the solution structure of $[Ln_2(L5)_3]^{6+}$ because of intricate and slow interconversion processes occurring on the NMR time scale,[13] a plausible explanation considers the shift of one ligand with respect to the two other strands according to the "vernier" mechanism (Scheme 2). This mechanism produces an unsaturated intermediate, in which only two neighboring nine-coordinate sites are available for complexation. Obviously, we cannot rule out mixtures containing more complicated structures, but the simple "box arrangement" depicted in Figure 1 is inadequate for rationalizing this complex.

Experimental Section

Solvents and Starting Materials. These were purchased from Fluka AG (Buchs, Switzerland) and Aldrich and used without further purification unless otherwise stated. The ligand bis{1-ethyl-2-[6′-(*N*,*N*-diethylcarbamoyl)pyridin-2′-yl]benzimidazol-5-yl}methane (L2) was prepared according to a literature procedure.[11] The triflate salts $Ln(CF_3SO_3)_3{\cdot}xH_2O$ (Ln = La−Lu, Y; x =1−4) were prepared from the corresponding oxides (Rhodia, 99.99%).[40] The Ln content of solid salts was determined by complexometric titrations with Titriplex III (Merck) in the presence of urotropine and xylene orange.[41] Acetonitrile was distilled over calcium hydride.

Preparation of the Complexes $[(Ln^1)_x(Ln^2)_{2-x}(L2)_3]^{6+}$ (Ln^1, Ln^2 = La, Nd, Sm, Eu, Yb, Lu, Y; x = 0−2). L2 (4.4 mg, 7×10^{-6} mol) and $Ln^1(CF_3SO_3)_3{\cdot}xH_2O$ and $Ln^2(CF_3SO_3)_3{\cdot}xH_2O$ in variable proportions (condition: $[Ln^1] + [Ln^2] = [Ln]_{tot} = 4.67 \times 10^{-6}$ M) were mixed in dichloromethane/acetonitrile (1:1, 2 mL). After stirring 3 h at room temperature, the solution was evaporated and dried under vacuum, and the solid residue was dissolved in CD_3CN (700 μL). The resulting solution was equilibrated for 48 h at 298 K prior to ^{1}H NMR

(39) Petoud, S.; Bünzli, J.-C. G.; Renaud, F.; Piguet, C.; Schenk, K. J.; Hopfgartner, G. *Inorg. Chem.* **1997**, *36*, 5750.

(40) Desreux, J.-F. In *Lanthanide Probes in Life, Chemical and Earth Sciences*; Bünzli, J.-C. G.; Choppin, G. R., Eds.; Elsevier Publishing Co: Amsterdam, 1989; Chapter 2, p 43.

(41) Schwarzenbach, G. *Complexometric Titrations*; Chapman & Hall: London, 1957; p 8.

measurement. For ESI-MS spectra, the final solutions were diluted with acetonitrile to give $[L2]_{tot} = 2 \times 10^{-4}$ M.

Spectroscopic and Analytical Measurements: Spectrophotometric titrations were performed in batch at 25 °C with a Perkin-Elmer Lambda 900 spectrometer using quartz cells of 0.1 cm path length. Acetonitrile solutions containing a total ligand concentration of 2×10^{-4} M, and variable concentrations of $Ln(CF_3SO_3)_3 \cdot xH_2O$ (Ln/L2 = 0.1−2.0, 35−40 samples) were left to equilibrate overnight at 298 K. The absorption spectrum of each sample was then recorded and transferred to the computer. Mathematical treatment of the spectrophotometric titrations was performed with factor analysis[16] and with the SPECFIT program.[17] ^{1}H NMR spectra were recorded on a Broadband Varian Gemini 300 MHz and Bruker DRX-500 MHz spectrometers at 298 K. Chemical shifts are given in ppm vs TMS. The relative proportion of each complex was determined by integration of the ^{1}H NMR signals at different Ln^1/Ln^2/L2 ratios. The associated stability constants were estimated from distributions simulated with the program MINEQL$^+$.[33] Pneumatically assisted electrospray (ESI-MS) mass spectra were recorded from 2×10^{-4} M acetonitrile solutions on a Finnigan SSQ 7000 instrument.

Calculations and Computational Details. Multilinear least-squares fits with the one-nucleus method (eq 5) were performed with Microsoft EXCEL software. The best least-squares lines according to the two-nuclei method (eq 10) were obtained by minimizing M where M is the sum along the lanthanide series ($j = 1$ to 9 corresponding to Ln = Pr, Nd, Eu, Tb, Dy, Ho, Er, Tm, Yb) of the square of the orthogonal distances to the line.[42] As a line is defined by its distance to the origin and by its unit normal, $\vec{n}$, we add to M the condition: $\varphi = (\vec{n} \cdot \vec{n}) - 1 = 0$ multiplied by a Lagrangian multiplier λ.[43] After equating all the partial derivatives of $m + \varphi$ with respect to n_x, n_y, and λ to zero, a system of equations is found which can be solved by using a software for symbolic computation,[44] thus leading to the best least-squares line.

Conclusion

This thorough thermodynamic and structural investigation of the self-assembly leading to $[Ln_2(L2)_3]^{6+}$ demonstrates that (i) the C_3-symmetrical *FAC*-$[Ln(L2)_3]^{3+}$ is the single thermodynamic intermediate formed in significant quantity in solution, (ii) the destruction of $[Ln_2(L2)_3]^{6+}$ in excess of metal (to give $[Ln_2(L2)_2]^{6+}$) is negligible for Ln/L2 ≤ 0.67 at millimolar concentrations, and (iii) a single D_3-symmetrical triple-stranded structure is observed for $[Ln_2(L2)_3]^{6+}$ along the complete lanthanide series (Figure 2). With these data at hand, it is possible to apply the simple *site-binding* thermodynamic model[14] for rationalizing the experimental macroscopic constants (Figure 9), which involves free energies of complexation around $\Delta G_t^\circ = -RT \ln(k_t^{Ln}) \approx -99(3)$ kJ mol^{-1} combined with intermetallic repulsion parameters around $\Delta E \approx 51(7)$ kJ mol^{-1} pointing to strong negative cooperativity (Table 4). Interestingly, ΔE can be simply interpreted as arising from the electrostatic repulsion between the two Ln(III) cations considered as point charges. Extension of this approach for the global rationalization of the assembly of the bimetallic $[Ln_2(L2)_3]^{6+}$ and the next homologous trimetallic $[Ln_3(L5)_3]^{9+}$ helicates shows that a satisfying fit requires the removal of the formation constants of the intermediate $[Ln_2(L5)_3]^{6+}$. This points to a specific structure for this elusive complex which is not correctly described by our "rigid box" model. Since the assembly process leading to $[Ln_3(L5)_3]^{9+}$ obeys repetitive statistical binding, we conclude that the free energy of complexation of the terminal N_6O_3 sites (ΔG_t°) and the repulsive interaction (ΔE) are similar for bimetallic and trimetallic helicates. Moreover, the free energy of complexation of the central site $\Delta G_c^\circ = -RT \ln(k_c^{Ln}) \approx -103(7)$ kJ mol^{-1} in $[Ln_3(L5)_3]^{9+}$ (Table 4) is only slightly more negative than that of the terminal site, in agreement with monometallic model complexes.[19] Consequently, the selective formation of heterometallic f−f helicates is very limited since it entirely depends on the different affinities of the two sites. The observation that the repulsive parameter $\Delta E_{Ln^1Ln^2}$ does not vary with the nature of the Ln^1/Ln^2 pair leads to the disappointing conclusion that allosteric effects in these rather rigid helicates remains too weak to be detected, a strongly limiting factor for designing pure heterometallic f−f complexes.[13] Compared with our previous partial analysis of the heterotrimetallic complexes $[(Ln^1)_x(Ln^2)_{3-x}(L5)_3]^{9+}$ ($x = 0-3$) in which we were compelled to fix $\Delta E = 0$,[13b] the current results bring a drastic improvement of the thermodynamic model, which provides physically interpretable parameters. However, the extraction of a reliable interaction parameter $\Delta E_{Ln^1Ln^2}$ strongly depends on (i) the incorporation in the fitting process of unsaturated intermediates for which some sites are vaccant and (ii) the simultaneous consideration of analogous complexes with different nuclearities displaying repetitive statistical binding. The first point has been addressed in this paper with the removal of the intermediate $[Ln_2(L5)_3]^{6+}$ whose structure does not fit our model. Therefore, only unsaturated intermediates exhibiting a well-defined and adapted structure as found for *FAC*-$[Ln(L2)_3]^{3+}$ must be considered. The second point relies on the increasing number of interactions between adjacent lanthanides which is 1 for bimetallic, 2 for trimetallic, 3 for tetrametallic helicates, etc. (i.e., $m - 1$ interactions in saturated one-dimensional polymers containing m lanthanides),[14] which provides sets of mathematically independent equations (k^2u for bimetallic, k^3u^2 for trimetallic, k^4u^3 for tetrametallic, and k^mu^{m-1} for m-metallic). In this contribution, the number of available formation constants $\log(\beta_{13}^{bi,Ln})$, $\log(\beta_{23}^{bi,LnLn})$, and $\log(\beta_{33}^{tri,LnLnLn})$ (9−11 data for each Ln^1/Ln^2 pair) is sufficient to obtain reliable values for terminal and central absolute affinities and for one intermetallic repulsion parameter. Further refinements involving (i) fitting processes which do not resort on unsaturated intermediates and (ii) the explicit consideration of a second repulsion parameter for two nonadjacent lanthanides ($\Delta E_{Ln^1Ln^2}^{1-3}$) will be only possible when the next homologous tetrametallic helicates (i.e., the combination of two terminal and two central sites) will become available.

Acknowledgment. We gratefully acknowledge Professor Gianfranco Ercolani (University of Roma) for helpful discussions. We thank Mr Luc-Alexis Leuthold and Professor Gérard Hopfgartner (University of Geneva) for recording selected ESI-MS data under ultrasmooth conditions and Ms Hélène Lartigue and Mr Bernard Bocquet for their technical assistance. This work is supported through grants from the Swiss National Science Foundation.

Supporting Information Available: Additional tables and figures. This material is available free of charge via the Internet at http://pubs.acs.org.

JA0483443

(42) Schomaker, V.; Waser, J.; Marsh, R. E.; Bergman, G. *Acta Crystallogr.* **1959**, *12*, 600.
(43) (a) Spiegel, M. R. *Advanced Calculus*, Schaum's outline series; McGraw-Hill: New York, 1974; Chapter 8, pp 164, 171−174. (b) Atkins, P. W. *Physical Chemistry*, 5th ed.; Oxford University Press: Oxford, 1994; pp A35−A36.
(44) *Maple 8*; Waterloo Maple Inc.: Waterloo ON N2L 5J2, Canada. www.maplesoft.com